OXFORD UNIVERSITY PRESS | Brain

Induction of immunological tolerance to myelinogenic glial-restricted progenitor allografts

Journal:	*Brain*
Manuscript ID	BRAIN-2018-01732.R3
Manuscript Type:	Original Article
Date Submitted by the Author:	22-Jun-2019
Complete List of Authors:	Li, Shen; Dalian Municipal Central Hospital, Neurology; Johns Hopkins University Oh, Byoung Chol; Johns Hopkins University Chu, Chengyan; Johns Hopkins University Arnold, Antje; Johns Hopkins University Jablonska, Anna; Johns Hopkins University Furtmuller, Georg; Johns Hopkins University Qin, Huamin; Johns Hopkins University Boltze, Johannes; University of Warwick Magnus, Tim; University of Hamburg Ludewig, Peter; University of Hamburg Janowski, Miroslaw; Johns Hopkins University Brandacher, Gerald; Johns Hopkins University Walczak, Piotr; Johns Hopkins University
Subject category:	Multiple sclerosis and neuroinflammation
To search keyword list, use whole or part words followed by an *:	Remyelination < MULTIPLE SCLEROSIS AND NEUROINFLAMMATION, Stem cells < NEURODEGENERATION: CELLULAR AND MOLECULAR, Leukodystrophy < MULTIPLE SCLEROSIS AND NEUROINFLAMMATION, Oligodendrocyte < MULTIPLE SCLEROSIS AND NEUROINFLAMMATION, Imaging methodology < SYSTEMS/DEVELOPMENT/PHYSIOLOGY

Induction of immunological tolerance to myelinogenic glial-restricted progenitor allografts

Authors: Shen Li,[1,2,3] Byoung Chol Oh,[4] Chengyan Chu,[2,3] Antje Arnold,[2,3] Anna Jablonska,[2,3] Georg J. Furtmüller,[4] Hua-Min Qin,[2,3] Johannes Boltze,[5] Tim Magnus,[6] Peter Ludewig,[6] Mirosław Janowski,[2,3] Gerald Brandacher[4] and Piotr Walczak[2,3]*

Affiliations:

[1]Neurology Department, Dalian Municipal Central Hospital affiliated to Dalian Medical University, Dalian, China.

[2]Division of MR Research, Russell H. Morgan Department of Radiology and Radiological Science, Johns Hopkins University School of Medicine, Baltimore, MD, USA.

[3]Cellular Imaging Section and Vascular Biology Program, Institute for Cell Engineering, Johns Hopkins University, Baltimore, MD, USA.

[4]Department of Plastic and Reconstructive Surgery, Vascularized Composite Allotransplantation (VCA) Laboratory, Johns Hopkins University School of Medicine, Baltimore, MD, USA.

[5]School of Life Sciences, University of Warwick, Coventry, CV4 7AL, United Kingdom.

[6]Neurology Department, University Medical Center Hamburg-Eppendorf, Hamburg, Germany.

*To whom correspondence should be addressed:

Piotr Walczak, MD/PhD, Associate Professor

Russell H. Morgan Department of Radiology and Radiological Science

Johns Hopkins University, 733 N Broadway, 647 MRB, Baltimore, MD, 21205

Phone: +1-443-287-5615

E-mail: pwalczak@mri.jhu.edu

Running title: Tolerance induction to GRP allografts

Abbreviated summary

White matter repair through allotransplantation of glial progenitors is now feasible in immune-deficient animals. However, immunological barrier precludes its clinical translation. We describe a strategy based on costimulation blockade inducing immunological hyporesponsiveness and supporting long-term functionality of allotransplanted myelinating oligodendrocytes.

Abstract

The immunological barrier currently precludes the clinical utilization of allogeneic stem cells. Although glial-restricted progenitors have become attractive candidates to treat a wide variety of neurological diseases, their survival in immunocompetent recipients is limited. In this study, we adopted a short-term, systemically applicable costimulation blockade-based strategy using CTLA4-Ig and anti-CD154 antibodies to modulate T cell activation in the context of allogeneic glial-restricted progenitor transplantation. We found that costimulation blockade successfully prevented rejection of allogeneic glial-restricted progenitors from immunocompetent mouse brains. The long-term engrafted glial-restricted progenitors myelinated dysmyelinated adult mouse brains within one month. Furthermore, we identified a set of plasma miRNAs whose levels specifically correlated to the dynamic changes of immunoreactivity and as such could serve as biomarkers for graft rejection or tolerance. We put forward a successful strategy to induce alloantigen-specific hyporesponsiveness towards stem cells in the central nervous system, which will foster effective therapeutic application of allogeneic stem cells.

Keywords

glial-restricted progenitors; costimulation blockade; myelination; immunological tolerance; transplantation

Abbreviations

4', 6-diamidino-2-phenylindole (DAPI); antigen presenting cells (APCs); bioluminescent imaging (BLI); blood brain barrier (BBB); *C57*BL/6 albino (B6); central nervous system (CNS); costimulation blockade (CoB); Dendritic cells (DC); fibroblast growth factor receptor (FGFR); glial-restricted progenitors (GRP); green fluorescent protein (GFP); human glial-restricted progenitors (hGRP); *in situ* hybridization (ISH); mouse glial-restricted progenitors (mGRP); myelin basic protein (MBP); phosphate buffer saline (PBS); post operation day (POD); proteolipid protein (PLP); regulatory T cell (Treg).

Introduction

Neurological disorders are the most compelling targets of cell-based therapy due to the very limited capacity of the central nervous system (CNS) to undergo spontaneous regeneration. This particularly accounts for glial diseases, as the initially preserved neuronal cytoarchitecture is believed to foster white matter repair (Boltze *et al.*, 2017). A broad variety of stem cell populations being capable of differentiating into oligodendrocytes including neural and oligodendrocyte progenitor cells, as well as glial-restricted progenitors (GRPs) have been investigated (Goldman, 2016). Moreover, oligodendrocytes directly derived from induced pluripotent stem cells, were shown to rapidly myelinate the newborn and adult CNS (Ehrlich *et al.*, 2017).

GRPs arise from neural stem cells and can differentiate into both oligodendrocytes and astrocytes under appropriate conditions (Rao and Mayer-Proschel, 1997; Rao *et al.*, 1998). Apart from leukodystrophies or multiple sclerosis, GRPs become promising candidates to treat a wide variety of neurological diseases (Goldman *et al.*, 2012; Goldman, 2016). Human GRPs (hGRPs) were shown to extensively migrate and myelinate the congenitally dysmyelinated newborn mouse brains and prolong the lifespan of the animals (Windrem *et al.*, 2004; Windrem *et al.*, 2008; Wang *et al.*, 2013; Lyczek *et al.*, 2017). These cells also preserve electrophysiological function in focal inflammatory spinal cord demyelination (Walczak *et al.*, 2011), support regeneration after spinal cord injury (Haas and Fischer, 2013), replenish depleted precursor pools, generate new myelin, and reverse radiation-induced behavioral defects in adult rats (Piao *et al.*, 2015).

Since cell treatments in future clinical scenarios will require very well-defined, thoroughly characterized, and standardized cell populations, the use of allogeneic grafts is believed to be the most likely approach. This is also advantageous when treating inherited diseases and acute injury

for which autologous cell generation and differentiation paradigms are not suitable. However, to date, the immunological barrier represents an unsurmountable challenge to widespread clinical application of allogeneic cells. In case of GRPs, robust rejection in less than three weeks after transplantation into white matter of immunocompetent adult recipients (Janowski *et al.*, 2014; Srivastava *et al.*, 2016) strongly limits GRP migration potential and therapeutic effects, so far demanding conventional immunosuppression regimens. Besides their low efficacy, risk of infection and tumor formation, immunosuppression-inherent effects, as well as associated cellular and systemic toxicities complicate preclinical studies and preclude successful clinical translation (Diehl *et al.*, 2017) of GRP-based treatments. Thus, novel immunomodulatory strategies are imperative.

Since T cells play a central role in the immune response toward allografts, an emerging immunomodulatory strategy targets costimulatory molecules involved in T cell activation (Verbinnen *et al.*, 2010; Kinnear *et al.*, 2013; Marino *et al.*, 2016). One of the most important costimulatory interactions are that of CD80/CD86 found on antigen presenting cells (APCs) interacting with CD28 located on T cells, and CD40 on APCs engaging CD154 on T cells (Lafferty *et al.*, 1983). CTLA4-Ig blocks the CD80/CD86-CD28 interaction. It prevents complete T cell activation with consecutive T cell anergy, thus protecting allografts in various small and large animal solid organ (Shiraishi *et al.*, 2002; Graves *et al.*, 2009) and cell transplantation models (Lenschow *et al.*, 1992). The concept has been successfully introduced into the clinic (Masson *et al.*, 2014). In addition, despite some initial setbacks, preclinical studies have demonstrated the potency of anti-CD154 antibody (MR-1) treatment targeting the CD40-CD154 axis for allograft rejection prevention (Webber and Vincenti, 2016). The combination of CTLA4-Ig and MR-1 has also been shown to induce long-term survival of skin and cardiac allografts (Larsen *et al.*, 1996) as

well as human embryonic stem cell-derived pancreatic endoderm xenografts in rodents (Szot *et al.*, 2015). However, it remains largely unknown whether the blood brain barrier (BBB) and microglial response may limit systemic costimulation blockade-based tolerance induction for allogeneic GRPs using CTLA4-Ig and MR-1.

One of the key obstacles in clinical translation of cell therapies is the lack of biomarkers that could indicate the status of transplanted cells (Bohmig *et al.*, 2010). Cellular imaging offers limited sensitivity and specificity (Berman *et al.*, 2011), so there is growing interest in exploiting miRNAs, lipids or proteins as blood biomarkers for intracerebral graft surveillance (Hamdorf *et al.*, 2017). MiRNAs are small, non-coding RNAs that act as key regulators of B- and T-cell differentiation, maturation, and proliferation. They also play a role in regulatory T cell (Treg) function and antigen signaling (Hoefig and Heissmeyer, 2008; Gaudet *et al.*, 2017). Their sensitivity, conserved expression and relative tissue specificity have triggered their potential utility as biomarkers for neuroinflammation (Hoefig and Heissmeyer, 2008; Gaudet *et al.*, 2017; Sajja *et al.*, 2017).

In the present study, we transplanted fully histocompatibility complex-mismatched GRP allografts into the mouse brain parenchyma and studied allograft survival and function by non-invasive imaging techniques and histological investigation. We showed that short-term costimulation blockade induced indefinite engraftment of GRP allografts in the mouse CNS. Moreover, several classes of circulating miRNAs were identified to be sensitive biomarkers for graft rejection/acceptance.

Materials and methods

Mice

Five/one cohorts of immunocompetent *C57*BL/6 albino (B6, male, 8-week-old, Jackson Laboratory) mice were used for allogeneic/xenogeneic GRP survival studies. Two cohorts of genetically dysmyelinated shiverer (male, 6-week-old, Jackson Laboratory) mice were included to examine the myelination capacity of allogeneic mouse GRPs (mGRPs) in adult brains treated with costimulation blockade (CoB). Immunodeficient, graft-accepting mice served as controls for cell or transplantation-related failures (scid mice control for B6 mice, and shiverer-rag2 mice control for shiverer mice). Every cohort of animals contained three groups: immunocompetent animals+CoB group, immunocompetent animals+phosphate buffer saline (PBS, control group), and immunodeficient animals (n=5/group). Detailed animal assignment, measurements, and dropouts are listed in Table 1. Drop-outs were not replaced. All mice were micro-chipped, randomly assigned into different groups, as well as manipulated and analyzed in a blinded manner. Animals were housed under an artificial light-dark (12 h/12 h) cycle and had access to food and water *ad libitum*.

Isolation and characterization of GRPs

Allogeneic GRPs were isolated from the spinal cord of a proteolipid protein (PLP)-green fluorescent protein (GFP) (for detection of differentiated oligodendrocytes)/β-actin-luciferase (for detection of engrafted cells *via* bioluminescent imaging) transgenic mouse strain at embryonic day 13.5 as described (Phillips *et al.*, 2012). Cells were maintained in serum-free Dulbecco's modified Eagle's medium (DMEM)/F12 (Life Technologies) supplemented with N2 (Life Technologies),

B27 (Life Technologies), bovine serum albumin (Sigma-Aldrich), heparin (Sigma-Aldrich), and basic fibroblast growth factor (bFGF, PeproTech) (Lepore *et al.*, 2006).

Primary hGRPs were derived from midgestation fetuses and thoroughly characterized as described elsewhere (Sandrock *et al.*, 2010) (Q Therapeutics). Cells were immortalized using lentivirus encoding the SV40 large T-antigen, and were selected with puromycin. They were maintained in serum-free DMEM/F12 medium supplemented with N2, B27, bovine serum albumin, and bFGF (Janowski *et al.*, 2013). Without hGRP indication, transplantations were performed with mGRPs.

Allogeneic mGRPs were characterized immunocytochemically. Briefly, cells were fixed in 4% paraformaldehyde for 20 min, blocked by 10% donkey serum in 0.1% Triton X-100-PBS for 2 h at room temperature. Cells were incubated with appropriate dilutions of primary antibodies in blocking solution overnight at 4°C, rinsed with PBS, and incubated with corresponding secondary antibodies (Alexa Fluro-594, Life Technologies-A11058) in blocking buffer for 1 h at room temperature. The culture was rinsed three times with PBS, counterstained with 4', 6-diamidino-2-phenylindole (DAPI, Sigma-Aldrich-D9542, 5 μg/ml), and imaged using a Zeiss AX10 fluorescence microscope. Primary antibodies were: anti-PDGFRα (1:1000, Abcam-ab61219), anti-A2B5 (1:500, Life Technologies-433110), anti-Olig1 (1:500, Millipore-AB15620), anti-Olig2 (1:500, Millipore-AB9610), anti-NG2 (1:500, Millipore-AB5320), anti-MBP (1:1000, AbD Serotec-MCA409S), anti-GFAP (1:1000, DAKO-Z0334), anti-Iba1 (1:500, Wako-SAN3725), anti-CD11b (1:500, BioLegend-101202), anti-βIII-Tubulin (1:500, Covance-PRB-435P), anti-Nestin (1:500, Millipore-MAB535), anti-CXCR4 (1:300, Abcam-ab1670), and anti-FGFR1 (1:200, Cell Signaling Technology-9740).

Cell transplantation

Anesthesia was induced with 5% isoflurane and maintained with 2% isoflurane in room air and oxygen mixed at 3:1 ratio. Mice were shaved and stabilized in a Cunningham adaptor mounted on a stereotactic frame (both Stoelting). A 7.0-mm skin incision was made along the midline of the skull. The skull bone was carefully exposed and Bregma was identified. A burr hole was placed according to the targets (B6 and scid mice: AP=1.7 mm; ML=0.7 mm; DV=2.0 mm). Cells were loaded into a 10-µl gastight Hamilton syringe (#1701) with an attached 31-gauge needle (Hamilton) and lowered into the brain according to the coordinates. Four microliters of mGRP suspension (100,000 cells/µl in PBS) were injected at a rate of 1 µl/min using a nano-injector (Stoelting). The needle was kept in place for 2 min after injection to minimize backflow and was then withdrawn slowly. The syringe was removed and the wound was closed with sutures (Silk 3.0; Ethicon). Shiverer and shiverer-rag2 mice received three injections targeting the corpus callosum to investigate the myelination capacity with 3 µl of mGRPs each through one hole (AP=0 mm; ML=2.1 mm). The first injection was placed vertically with a 2.0-mm depth. The second injection had a 30° angle with the vertical line to the rostral. The third injection had a 45° angle with the vertical line to the caudal.

Costimulation blockade

CTLA4-Ig (ORENCIA, Bristol-Myers Squibb Company) was intraperitoneally administered at 500 µg/mouse in combination with 500 µg/mouse anti-CD154 mAbs (MR-1, BioXCell) at the time of transplantation and on post operation day (POD)2, 4, and 6, based on previous tolerance induction protocol in rodents (Larsen *et al.*, 1996; Szot *et al.*, 2015). Booster CoB mice received additional 500 µg/mouse CTLA4-Ig on POD30, 60, and 90.

Bioluminescent imaging (BLI) of transplanted GRPs in vivo

Bioluminescence images were acquired using an IVIS Spectrum/CT instrument. Animals were anesthetized by 2% isoflurane gas in oxygen, with 150 mg/kg D-luciferin (Gold Biotechnology) injected intraperitoneally. BLI was initiated the day after cell transplantation and continued on POD3, 7, 10, and then weekly until the endpoints. Images were quantified by drawing regions of interest (ROIs) over the mouse brains or backs, with data expressed as total photon flux (photons/s). Cell survival curves were generated as logistic graphs. A drop in BLI signal to the background level (signal generated by other parts of the body) was interpreted as rejection of transplanted cells (Janowski *et al.*, 2014; Srivastava *et al.*, 2016).

Adoptive transfer experiment

For adoptive transfers, single-cell suspensions were prepared from the spleen of B6 mice (one pair of 154-day post intracerebral mGRP transplanted CoB and control B6 mice, one age-matched naïve mouse). Two million purified T cells were injected into the retro-orbital blood sinus of scid mice (5 groups, n=4/group). Four days later, one million mGRPs were subcutaneously transplanted into the back of each scid mouse and the survival of allografts was monitored by BLI.

Mixed lymphocyte reaction (MLR)

T cell isolation was performed *via* negative selection for B cells, NK cells, monocytes/macrophages, dendritic cells, erythrocytes, and granulocytes from splenocytes of recipient mice using magnetic bead sorting. Briefly, splenocytes were incubated with purified rat anti-mouse B220, Gr-1, TER-119, I-A/I-E, CD11b, and CD16/32 (eBioscience) and subsequently

incubated with anti-rat IgG Dynabeads (Dynabeads® Untouched™ Mouse T Cells, Life technologies) leading to a T cell enriched population following magnetic selection. Two micromole of CFSE (Vybrant CFSE SE cell tracer kit, Life technologies) was applied for tracking proliferation.

Dendritic cells (DC) were generated from both donor matched (FVBN) and third party derived (Balb/c) bone marrow after cultured for 7 days with IL-4 and GM-CSF in a 37°C incubator. DCs were activated with a 1:5000 diluted lipopolysaccharides 24 h prior to MLR plating. CD11c-positive DCs were then isolated using positive magnetic sorting according to the manufacturer's protocol (Mouse CD11c Positive Selection Kit, STEMCELL Technologies).

CFSE-labeled T cells and DCs were cultured together with either intact mGRPs or ultrasonicly minced mGRPs for 4 d in 37°C, collected, and stained with Fixable Viability Dye (eBioscience) according to the manufacturer's protocol. Samples were stained for CD4 and CD8 and acquired on a LSRII flow cytometry (BD Biosicence). Data were analyzed using FlowJo software (Tree Star Inc.) and normalized to the proliferation of naïve cells within each individual experiment.

Cytokine assay

The Bioplex 200 platform (Biorad) was used to efficiently determine the concentration (in pg/ml) of multiple target proteins in mGRP-engrafted B6 and scid mouse serum, according to the manufacturer's protocols using the supplied cytokine standards. The concentration was determined using a 5-parameter log curve fit using the supplied software. The Mouse Group I 23 plex panel was used to measure IL-1α, IL-1β, IL-2, IL-3, IL-4, IL-5, IL-6, IL-9, IL-10, IL-12 (p40), IL-12

(p70), IL-13, IL-17A, Eotaxin, G-CSF, GM-CSF, IFNγ, KC, MCP-1, MIP-1α, MIP-1β, RANTES and TNFα. The levels of TGFβ were assessed separately (Biorad).

Treg analysis

Intracellular cytokine staining was performed according to the manufacturer's protocol. Briefly, cells were washed, stained for surface markers, fixed with BD Cytofix/Cytoperm, permeabilized, and incubated with antibodies against intracellular markers for 40 min on ice. Flow acquisition was performed on a LSRII flow cytometry (BD Biosicence), and data were analyzed using FlowJo software (Tree Star Inc.). Fluorochrome-tagged antibodies were: CD4-PB (eBioscience-RM4-5), CD8-FITC (BD Pharmingen-53-6.7), CD25-PE (BD Pharmingen-PC61), and FoxP3-PerCP-Cy5.5 (eBioscience-JFK-16s).

MiRNA analysis

RNA isolation was performed with mouse plasma using a miRCURY RNA Isolation Kit Biofluids (Exiqon) according to the manufacturer's protocol. For isolation, 100 µl of plasma was used and one step of DNase treatment was added. RNA Spike-in U6 template was added to the mixture as an internal control. Purity and quantity of the isolated miRNA were measured with NanoDrop photometry. The RNA samples were diluted with nuclease-free water to concentration of 5 ng/µl and 2 µl of RNA was used for synthesis of first-strand cDNA using a miRCURY LNA Universal RT microRNA PCR kit (Exiqon) according to the manufacturer's protocol. Real-Time PCR was performed with ExiLENT SYBR-Green master mix with LNA Primers specific for miRNAs (let 7a/7c, miR-125b, miR-146, miR-150, miR-223) (Exiqon). Results determined the changes in

steady-state miRNA levels of a gene across multiple samples, and were expressed relatively to the pre-transplantation levels and the levels of an internal control RNA.

Supplementary methods

The Supplementary Materials provide further details for immunohistochemical analysis, MRI, erichrome cyanin staining, transmission electron microscopy and g-ratio measurement, and miRNA *in situ* hybridization.

Statistical analysis

Data are expressed as mean ± standard deviation (SD) or median [interquartile range]. No animals (despite dropouts) or samples were excluded from the analysis. For investigation of GRP survival and cytokine assay, regression analysis was reported as type III tests of fixed effects, with the lowest mean square (LMS) difference test used for comparison between means (PROC MIXED, SAS 9.2). A coefficient of determination was calculated, and the BLI data were subjected to logistic transformation to maximize the model fit. CD45, Iba-1 and CD68 immunohistochemical analysis and GFP-MBP co-localization were assessed using a 2-sided Kruskal-Wallis test with Bonferroni's adjustment. One way ANOVA with Bonferroni's adjustment was used for T cell infiltration and miRNA analysis, and an independent t-test (2-tailed) was performed for mixed lymphocyte reaction and Treg analysis. Mann-Whitney test for g-ratio analysis (SPSS 22.0). Sample size, statistical methods, and p values are given in figure legends. Significance was defined at $p<0.05$.

Study approval

All experimental procedures were in accordance with the guidance provided in the Rodent Survival Surgery Manual and were approved by Johns Hopkins Institutional Animal Care and Use Committee (MO14182).

Data availability

The authors declare that all data supporting the findings of this study are available within the article and its Supplementary Materials, or from the authors upon reasonable request.

Results

Costimulation blockade induces engraftment of GRP allografts in immunocompetent adult B6 mice.

Allogeneic GRP survival was first assessed in immunocompetent adult B6 mouse brains and the phenotypic identity of mGRPs was verified by immunocytochemistry with different cell lineage markers. These cells expressed high levels of A2B5, PDGFRα, NG2, Nestin, Olig1 and Olig2. They were negative for Iba-1, CD11b, β-tubulin and MBP. Some cells were GFAP-positive reflecting the bidirectional differentiation capacity of GRPs (Rao *et al.*, 1998) (Supplementary Fig. 1). Membrane proteins PDGFRα (Tsai *et al.*, 2016), NG2 (Biname *et al.*, 2013), PLP (Harlow *et al.*, 2014; Harlow *et al.*, 2015) (Supplementary Fig. 1), CXCR4 (Tsai *et al.*, 2016), and FGFR (Bribian *et al.*, 2006) (Supplementary Fig. 2) were reported to mediate oligodendrocyte precursor migration and were positive in mGRPs.

After mGRP transplantation to the forceps minor of the corpus callosum, a location known for its capacity of robustly rejecting GRP allografts (Janowski *et al.*, 2014), scid, CoB and control mice all displayed BLI signal decline within the first three weeks. There was a complete signal loss in control mice, but scid and CoB mice exhibited a persistent mGRP signal until the endpoint of the study (203 days). Both scid and CoB groups showed a statistically significant difference from control group ($p<0.05$) from POD14 onwards (Fig. 1A). To investigate whether additional CTLA4-Ig-based treatment may enhance the survival of mGRPs, five randomly selected CoB mice (booster group) received monthly CTLA4-Ig treatment, mimicking a clinically effective immunosuppression maintenance strategy (Kirk *et al.*, 2014). No difference in graft survival was observed between non-booster (CTLA4-Ig and MR-1 treatment on POD0, 2, 4 and 6) and booster (additional CTLA4-Ig treatment on POD30, 60, 90) groups (Supplementary Fig. 3).

To test systemic hyporesponsiveness against donor antigens, secondary subcutaneous injections of mGRPs isolated from the donor of the original brain grafts were performed after 120 days of primary intracerebral grafting in randomly selected CoB (n=3) and scid mice (n=3). Resembling the survival curve of primary intracerebral transplantation, naïve B6 controls (n=5) rejected subcutaneously transplanted mGRPs within three weeks. Scid and CoB mice, however, accepted both primary (brain) and secondary (subcutaneous) mGRP allografts (Fig. 1B). After 17 days of secondary subcutaneous transplantation (POD137 of intracerebral transplantation), BLI signals were significantly higher in both CoB and scid mice compared to naïve controls ($p<0.001$ on all time-points examined). Signals were detectable for 83 days after secondary transplantation until animals were sacrificed for post-mortem assessment (=overall 203 days of investigation, the endpoint of the study) (Fig. 1B, C).

Adoptive-T cell transfer experiments were performed to provide evidence for systemic hyporesponsiveness rather than sequestration of the grafts behind the BBB. T cells were isolated from a naïve B6 mouse, CoB, and control mice (POD154 of intracerebral mGRP transplantation, indefinite engraftment was regarded to be established), and were retro-orbitally injected into scid mice with different donor configurations (n=4/group). Four days later, mGRPs were subcutaneously transplanted to the back of these scid mice. BLI revealed that scid mice receiving naïve T cells showed a significant drop in BLI signal 7 days after mGRP transplantation, indicating a fast rejection process. Scid mice receiving control T cells exhibited more robust rejection indicating a priming effect upon mGRP inoculation. However, the BLI signals in scid mice receiving T cells from the CoB-treated mouse was maintained, demonstrating donor-specific hyporesponsiveness towards mGRPs primarily engrafted in the brain (Fig. 1D).

Histological examination performed to confirm cell survival and identification revealed strong expression of GFP under the oligodendrocyte-specific PLP promoter in CoB and scid mouse brains (POD154). Elaborate processes indicated maturation of grafted cells towards myelinating oligodendrocytes. There was no leukocyte recruitment in CoB brains as examined by CD45 staining (Fig. 1E).

Human GRPs were transplanted into B6 brains to investigate whether costimulation blockade was effective in protecting intracerebral xenografts. Earlier rejection of hGRPs than mGRPs was observed in control group starting from POD3, and was completed within two weeks post transplantation. In contrast, hGRPs survived well in CoB group by POD19, the endpoint of the study. There was no difference in hGRP survival between CoB and scid mice (Supplementary Fig. 4).

Costimulation blockade prevents immune reaction against GRP allografts.

To characterize the underlying immune response allowing for allogeneic GRP survival, the extent and type of cellular infiltrate at the location of intracerebral mGRP injection were evaluated by panleukocyte marker CD45, T cell marker CD3, microglial/macrophage marker Iba-1, and active phagocyte marker CD68 immunostaining. Mouse brains were harvested at the peak of rejection as monitored by rapidly diminishing BLI signals in the control group (POD19). As expected, intense immune cell infiltration was detected around the mGRP grafts in control brains, yet only limited immune cell recruitment was observed in scid and CoB-treated mouse brains (Fig. 2A). Quantitative analysis of CD45 infiltration by both CD45 positive area (Fig. 2B, C) and fluorescent intensity (Fig. 2B, D) revealed statistically significant differences between control and CoB group, the latter being at a comparative level to scid brains. Of note, mGRPs in control brains were clotted and exhibited necrotic morphology on POD19. In contrast, mGRPs in CoB-treated and scid mouse

brains appeared vital and extended multiple processes, suggesting the integration of grafts into the host brain structure (Fig. 2A and Supplementary Fig. 5).

Excellent graft survival in scid mice revealed the pivotal role that T cells play in immune rejection. Investigations on infiltration of the graft site by T cells were performed after intracerebral mGRP transplantation. Not surprising, a large number of CD3-positive cells were detected encompassing the grafts in the control group. In contrast, T cells were absent in CoB and scid groups as shown by quantitative analysis of cell counts (Fig. 2E, F). Accordingly, the Foxp3 staining was negative in CoB and scid brains (data not shown). Interestingly, the proportion of $Foxp3^+$ Tregs among $CD4^+$ T cells was significantly decreased in CoB spleen on POD5 as compared to control mice, which further decreased on POD12 (Supplementary Fig. 6). These data implied that the CoB-mediated immunomodulation was not Treg dependent.

Quantitative analysis of Iba-1 immunofluorescence at POD19 was performed to identify local inflammatory and immune reactions. Although Iba-1 intensity was not different between CoB and control groups (Fig. 3A, B), control brains had a much larger Iba-1-positive area surrounding the grafts compared to CoB and scid brains (Fig. 3C) being indicative of extensive phagocyte recruitment to control brains, which was abrogated by CoB treatment. Next, we further analyzed the phagocytic activity by CD68 fluorescent staining, which revealed significantly weaker intensity (Fig. 3D, E) and smaller areas (Fig. 3D, F) in CoB brains than in control brains. There was no difference in CD68 intensity and positive area between CoB and scid brains.

We further analyzed the peripheral cytokine profiles by a high throughput multiplex bead-based immunoassay to investigate the molecular mechanism mediating allograft acceptance (from early graft implantation to complete rejection in control mice). Out of 20 cytokines that were within the detection range, both the pro-inflammatory IL-1β, IL-5, IL-12(p70), MCP-1, MIP-1β, MIP-1α, IL-

17, and TNFα, and anti-inflammatory IL-10 and IL-13 were increased in CoB sera as compared to control sera on POD5 while IL-1α (pro-inflammation) levels were decreased in CoB sera. The differences between CoB and control mice regarding these cytokine levels diminished gradually on POD11 and POD17. The expression levels of IL-1β, IL-12(p70), and MIP-1β in control mice exceeded those in CoB mouse on POD25, and there was more chemokine RANTES in control sera than in CoB sera on POD25 indicating a pro-inflammatory transition in the control group. Moreover, the dynamic changes of IL-12(p70) in CoB mice resembled the scid pattern, but was different from the control levels which were low in the early post-implantation period, but gradually elevated and exceeded the CoB and scid levels by POD17 and 25, respectively. The levels of IL-12(p40), antagonist of IL-12(p70), were higher in control mice when compared to CoB mice at all time-points examined. IL-10, a major anti-inflammatory cytokine, was expressed at similar and elevated levels in CoB and scid mice on POD5 as compared to control mice (Supplementary Fig. 7, a clustered heatmap shown in Supplementary Fig. 8). These results indicated that the transplantation induced pro-inflammatory cytokine profile was mitigated by costimulation blockade.

Costimulation blockade-protected allogeneic GRPs myelinate adult shiverer mouse brains.

We further aimed to utilize the costimulation blockade strategy for allogeneic GRP treatment. MGRPs were injected into unilateral corpus callosum of adult myelin basic protein (MBP) deficient, thus congenitally hypomyelinated, shiverer (Lachapelle *et al.*, 1983) and immunodeficient shiverer (shiverer-rag2-/-, shiverer-rag2) mice. Longitudinal BLI revealed that mGRPs could not survive in immunocompetent shiverer mice and were depleted from the host brains within three weeks after transplantation, replicating the dynamics shown in our wild-type animal mGRP transplant

experiments (Fig. 1). Despite an initial cell loss in shiverer-CoB and shiverer-rag2 mice during the first three weeks after transplantation, mGRP signals were consistently detected until the end of the natural lifespan of shiverer mice (POD90). Statistical differences were observed between shiverer-control and shiverer-CoB groups in mGRP survival from POD14, with no further changes in BLI thereafter. In addition, the survival of mGRPs in shiverer-CoB mice was at comparable levels to that in immunodeficient shiverer-rag2 mice ($p>0.05$ at all time-points examined, Fig. 4A, B).

Mixed lymphocyte reactions were carried out to assess systemic T cell responsiveness upon costimulation blockade in shiverer mice on POD33. T cells were isolated from naïve shiverer, shiverer-CoB and shiverer-control mouse spleen (n=3/group) and cultured together with mGRPs (either intact or minced (to expose the intracellular antigens)) in the presence of either donor-matched allogeneic or third party derived dendritic cells serving as APCs. Both $CD4^+$ and $CD8^+$ T cells obtained from shiverer-CoB mice showed reduced proliferation when co-cultured with either intact or minced mGRPs in the presence of donor-matched or third party derived APCs as compared to shiverer-control levels. These data indicated that CoB induces T cell hyporesponsiveness against mGRP antigens both *in vivo* and *in vitro* (Fig. 4C, D).

Shiverer mice were subjected to MR scanning to non-invasively visualize the behavior of allogeneic GRPs *in vivo* and to investigate whether immunoprotected mGRPs integrate functionally into the hosts and generate mature myelin. While T2-weighted images showed excellent white-gray matter contrast in age-matched rag2-/- mice (Fig. 5A), the T2 contrast was practically absent (except for the vertical needle tracts) in shiverer-control mice on POD60 and POD90. There was no visible discrimination of white matter on POD60 in shiverer-CoB and shiverer-rag2 brains, neither. However, on POD90, shiverer-CoB and shiverer-rag2 brains

displayed hypointensities along the corpus callosum in the injection side in T2 weighted images indicating mGRP-induced myelination (Fig. 5B).

Next, we examined MBP immunostaining in mGRP transplanted shiverer mouse brains. On POD33, allogeneic GRPs survived and migrated along the corpus callosum in shiverer-CoB mouse brains, and MBP was re-expressed in shiverers being co-localized with PLP-GFP-positive mGRPs (co-localization parameters shown in Supplementary Table 1). Furthermore, mGRP derived oligodendrocytes and MBP expression widely spread across the injection sites and the ipsilateral corpus callosum in shiverer-CoB and shiverer-rag2 brains on POD90. On the contrary, there was neither allogeneic GRPs nor MBP expression in shiverer-control brains on POD90 (Fig. 5C, D).

Erichrome cyanin staining was performed to examine the hydrophobic compartment within myelin proteins and lipid molecules to verify the myelin integrity in mGRP-engrafted shiverer mice. Although MBP could be detected on POD33 in shiverer-CoB mice, erichrome staining was negative in these animals indicating that myelin was not yet generated. On POD73 and POD90, mature myelin formation could be verified by erichrome-positive staining along the ipsilateral corpus callosum in shiverer-CoB and shiverer-rag2 mice (Fig. 6A).

Transmission electron microscopy was carried out to confirm allogeneic mGRP-derived myelin formation in shiverer mice. Numerous normally compact myelin sheaths were observed in shiverer-CoB mouse corpus callosum on POD90. There were few myelinated axons with thin myelin sheaths being loosely wrapped in shiverer-control brains (Fig. 6B). The thickness of myelin, assessed by g-ratio, was 0.9214[0.873-0.9482] and 0.8071[0.706-0.898] in shiverer-control and shiverer-CoB brains, respectively ($p<0.0001$). This is consistent with previous reports (Gansmuller *et al.*, 1986).

Circulating miRNAs are potential biomarkers for early detection of graft status.

As costimulation blockade provided a new strategy for intracerebral graft acceptance, we compared the expression of several immunoreactivity-linked miRNAs (Hoefig and Heissmeyer, 2008; Schjenken *et al.*, 2016; Gaudet *et al.*, 2017) in CoB and control B6 mouse plasma after intracerebral mGRP transplantation to explore potential graft rejection/acceptance biomarkers. A number of miRNAs were differently expressed between control and CoB mice. For instance, MiR-146 was upregulated gradually in control B6 mice after mGRP transplantation, reaching an approximately 17/12-fold expression level by POD12/19, the time of active rejection. However, in CoB mice, miR-146 levels were clearly downregulated, reaching undetectable levels on POD5/12 and recovered to sham-transplantation levels on POD19. Likewise, MiR-223 was increasingly upregulated in graft-rejecting control mice with statistical difference between POD5 and POD12, while its expression decreased in CoB mice after POD2. The opposite trend was observed for Let 7a/7c for which expression steadily increased in CoB mice until POD19 with reduction observed in rejecting control mice until POD12. Levels returned to those observed in vehicle-transplanted mice when rejection was close to completion on POD19. While the expression of miR-150 did not show differences between different observation days in control mice, it was downregulated gradually in CoB group. The levels of miR-125b in the plasma decreased gradually in control mice from POD2 to POD12. Its levels in CoB mice remained lower than in control mice (Fig. 7B-F). The vehicle-transplanted CoB group and sham-operation group did not show temporal differences in these miRNA levels, which excluded the costimulation blockade or surgery induced miRNA changes. *In situ* hybridization revealed higher peri-graft miRNA-146 in control than in CoB brains (relative fluorescent intensity 1.551 vs. 1.000, $p<0.0001$), while neither higher expression nor inter-group difference were observed for miRNA-233 (Supplementary Fig. 9).

Discussion

Thus far, the use of allogeneic stem cells to restore cerebral cytostructure and function is precluded by a lack of efficacy due to graft rejection, as well as negative effects of required immunosuppression protocols in attempts ensuring graft survival. In the current study, combined costimulation blockade using CTLA4-Ig and MR-1 successfully prevented allograft rejection from adult mouse brains. Furthermore, immunoprotected allogeneic GRPs differentiated and initiated myelination in the dysmyelinated adult mouse brain within one month, which could potentially represent an attractive option for patients with dysmyelinating diseases. In addition, several microRNAs including miR-146, miR-223, and let 7a/7c were identified as promising graft acceptance/rejection biomarkers.

In modern transplantation medicine, immunomodulatory strategies have entered the clinical arena to achieve graft survival with reduced toxicity or even immunosuppression-free stages (Diehl *et al.*, 2017). Our study showed that costimulation blockade in immunocompetent hosts resulted in long-term allogeneic GRP survival matching that in immunodeficient mice. These results align well with previous reports on the prevention of rejection in small and large animal models of organ transplantation using CTLA4-Ig and MR-1 (Larsen *et al.*, 1996; Bluestone *et al.*, 2006; Gilson *et al.*, 2009; Szot *et al.*, 2015; Webber and Vincenti, 2016). Several cell transplantation studies used costimulation blockade approaches for intracerebral transplantation of human embryonic stem cell-derived neural stem cells with cell survival for up to 56 days after grafting (Pearl *et al.*, 2011). CTLA4-Ig has also been applied to prevent rejection of human $CD34^+$ hematopoietic cells. Good cell survival at 56 days was achieved when mice were injected with blocking antibodies over 27 days after grafting, but cells were rejected when treatment was maintained for only 13 days (Oh *et al.*, 2017). We successfully push forward this strategy and observe intracerebral mGRP survival

for more than 200 days with functional integration. However, while this study sought to investigate the survival and myelination capacity of allogeneic GRPs under the protection of costimulation blockade, we transplanted GRPs to unilateral corpus callosum, with the contralateral hemisphere serving as an internal control. The small amount of locally transplanted GRPs were not sufficient to rescue the phenotype of shiverer mice that exhibit global demyelination. The therapeutic dose as well as the optimal route of GRP transplantation await detailed investigation.

Costimulation blockade effectively prevented local immune reactions with significantly less phagocyte reactivity and T cell infiltration around the mGRP allografts in CoB-treated mice compared to untreated immunocompetent controls. However, it is important to expand our investigation into the nature of the immunomodulatory effects and answer whether costimulation blockade effects are elicited exclusively in the CNS or, alternatively, in a systemic fashion. This is particularly relevant since peripheral maladaptive immune responses are already in place in many demyelinating disorders such as MS. We showed that subcutaneous injection of donor-matched GRPs into recipients with primary, intracerebrally-engrafted GRPs resulted in good cell survival in the CoB group with rejection in the controls supporting a state of systemic hyporesponsivness rather than a protective effect of the BBB. This is important as otherwise any local BBB breach in the course of brain injury or inflammation could trigger rejection processes. Evidence of systemic tolerance is also encouraging in the context of repetitive therapeutic application of immunologically matched stem cells.

We have demonstrated here that CoB is also effective in protecting xenografted human GRPs. This is highly significant as it allows studying behavior of human cells in various available transgenic mouse models or disease systems where adaptive immunity plays important role such as stroke or multiple sclerosis. We have recently shown that similar strategy with CoB can be used for modeling

human glioblastoma in immunocompetent mice (Semenkow *et al.*, 2017) further demonstrating universal utility of this method.

Costimulation blockade induced dynamic changes in the serum cytokine network during systematic allograft acceptance. It has been reported that inhibition of CD28-B7 interaction could alter cytokine profiles from Th1 to Th2 (Lin *et al.*, 1997). Moreover, Th1 and Th2 cells were differentially regulated by CD28-B7 versus CD154-CD40 costimulation pathways *in vivo* (Kishimoto *et al.*, 2000). While the serum cytokine expression differences between CoB and control groups diminished gradually after initial elevation on both Th1 and Th2 cytokines in CoB group, IL-1β, IL-12(p70), RANTES and MIP-1β levels steadily increased in control group and exceeded the CoB levels at POD25. Together with IL-12(p40) expression, whose levels were sustained high in control group, transition to pattern of Th2 cytokine expression might be a major player mediating costimulation blockade dependent immune tolerance induction.

Although Tregs are important regulators for alloimmune responses (Adams *et al.*, 2016) in organ and cell transplantation (Camirand and Riella, 2017), the effects of costimulation blockade on Tregs is still unclear. It was assumed that co-stimulation blockade inhibits Treg survival and function (Adams *et al.*, 2016), and an *in-vitro* study showed that CTLA4-Ig inhibited Treg proliferation (Levitsky *et al.*, 2013). Tolerance induced by costimulation blockade for human embryonic stem-cell-derived pancreatic endoderm was shown to be independent on Tregs (Szot *et al.*, 2015). Flowcytometric analysis indicated that CTLA4-Ig did not induce Treg expansion in peripheral blood of transplanted patients (Chavez *et al.*, 2007). We show that GRP allografts were not negatively affected although Tregs were decreased in CoB-treated recipients. In addition, we could not detect infiltrating T cells as well as Foxp3 T cells into the CoB brain after GRP engraftment. Due to limited studies regarding Treg activities in the brain as well as across the BBB,

the role of systemic Treg cells on the intracerebral mGRP allografts needs further mechanistic studies.

This study yields highly encouraging results on potential peripheral surrogate miRNAs for graft rejection as their specific temporal pattern correlated with survival or rejection of allogeneic GRPs. In addition, our results are supported by previous studies showing that miR-223 and miR-146 were both overexpressed, while let 7 levels were downregulated, in renal biopsies with confirmed T-cell mediated acute rejection compared to normal allografted patients (Anglicheau *et al.*, 2009). In rat liver transplantation settings, miR-223 and miR-146 levels were also significantly increased in allografts with acute rejection (Hu *et al.*, 2013; Morita *et al.*, 2014). Moreover, MiR-223 levels were reported to be highly predictive of acute renal rejection and strongly linked to the intragraft expression of CD3 mRNA (Sui *et al.*, 2008; Betts *et al.*, 2014). MiR-146 and miR-223 are produced by activated macrophages and are key anti-inflammatory miRNAs (Gaudet *et al.*, 2017). Their upregulation during rejection may reflect a negative feedback for inflammatory responses. The increased intragraft miR-146 expression and good graft survival confirmed its tolerance promotion property. The Let 7 miRNA family promotes both anti- and pro-inflammatory actions (Gaudet *et al.*, 2017). The miR-125b-let 7c-miR-99a cluster buffers against aberrant self-renewal and differentiation of hematopoietic stem cells by simultaneously targeting TGFβ and WNT1 signaling and plays a role in the development of Th1 cells (Mehta and Baltimore, 2016). Thus, dynamic profiles of miRNAs could be evaluated as potential biomarkers for monitoring graft survival and may help to improve the overall prognosis of patients with neurological disorders undergoing GRP transplantation.

In conclusion, this study demonstrates the efficacy of a combined costimulation blockade-based immunomodulatory protocol to achieve survival and retain (re)myelination capacity of allogeneic

GRPs transplanted directly into the murine CNS. In addition, we show that miRNAs may represent a meaningful tool for monitoring allograft viability, specifically in anatomical areas inaccessible to conventional methods. These encouraging data may foster the advancement of allogeneic GRPs' potential to enhance functional recovery in dysmyelination disorders in both translational large animal models and humans.

Acknowledgments

We would like to thank Mary McAlister for editorial assistance.

Funding

This study was funded by NIH/NINDS R01NS091110, R01NS091100, R01NS102675, 2017-MSCRFD-3942.

Competing interests

The authors report no competing interests.

Supplementary Materials

Supplementary Methods

Immunohistochemical analysis

Mice were anesthetized and perfused intracardially with 5% sucrose followed by PBS-buffered 4% paraformaldehyde. Brains were taken out, postfixed overnight at 4°C in 4% paraformaldehyde, dehydrated in 30% sucrose (Sigma-Aldrich), snap-frozen, and cryosectioned (Thermo Scientific HM 550 Cryostat) into 30-µm coronal sections. Nonspecific binding was blocked by incubating with 10% donkey serum in 0.1% Triton X-100-PBS for 1 h at room temperature. Appropriate dilutions of primary antibodies were then applied in blocking solution overnight at 4°C. After three washes, the corresponding secondary antibodies (in blocking solution, Alexa Fluro-594, Life Technologies-A11058) were incubated for 1 h at room temperature. Sections were then rinsed with PBS, counterstained with DAPI, and mounted with aqueous non-fluorescence mounting medium (Immu-mount, Thermo Scientific). Images were acquired with a Zeiss AX10 fluorescence microscope using the same exposure time and quantified with Image J. Primary antibodies were: anti-CD45 (1:500, Serotec-MCA1388); anti-Iba-1 (1:250, Wako-SAN3725); anti-CD3 (1:200, R&D-MAB4841); anti-CD68 (1:100, Abcam-ab31630); anti-MBP (1:1000, Serotec-MCA409S); anti-human cytoplasmic marker STEM121 (1:250, StemCells-AB-121-U050). The co-localization parameters between GFP and MBP was analyzed using Image-Pro Plus 6.0.

MRI

In-vivo MRI was performed on a horizontal 11.7 Tesla MR scanner (Bruker Biospin) with a triple-axis gradient (maximum gradient strength=74 Gauss/cm). During imaging, mice were anesthetized

with 1% isoflurane in room air and oxygen mixed at 3:1 ratio *via* a vaporizer, and positioned in an animal holder containing circulating warm water (Bruker Biospin). Respiration was monitored *via* a pressure sensor (SAII, Stony Brook) and maintained at 40-60 breath/min. After imaging, animals recovered within 5 min.

Image acquisition was performed using a quadrature transmit volume coil (70-mm diameter) and a 4-channel mouse brain receive-only phased array coil (Bruker Biospin). Multi-slice T2-weighted images were acquired using the rapid acquisition with refocused echoes (RARE) sequence with an echo time (TE) of 50 ms, a repetition time (TR) of 3600 ms, four signal averages, echo train length of eight, field of view (FOV) of 15x15 mm, 32 slices, and a native resolution of 0.078x0.078x0.50 mm.

Erichrome cyanin staining

Slides were oven-dried at 50°C for 3 h, hydrated in 95% and 70% ethanol. After rinsing with distilled water twice, the sections were stained with an erichrome cyanine solution consisting of 0.4% $FeCl_3$, 0.2% erichrome cyanine (Sigma-Aldrich) and 0.5% H_2SO_4. Section development was performed by alternating exposure to 0.1% NH_4OH for 3-7 s and rinsing in distilled water for 30 s until the blue background was reduced and cells turned faintly pink but still had blue shading. After the last rinse in water, sections were dehydrated in 70%, 95%, and 100% ethanol (two changes), and three changes of xylene for 10 min each before being processed for microscopy.

Transmission electron microscopy and g-ratio measurement

Perfused shiverer mouse brains were placed under a fluorescent dissection microscope. A 3-mm diameter cube was dissected from the mGRP transplanted corpus callosum and fixed in 4% glutaraldehyde following postfixation in OsO_4, and embedded in Epon. Thin sections of 70 nm were stained with citrate/uranyl acetate as recently described (Lyczek *et al.*, 2017). Images were acquired using a Zeiss Libra transmission electron microscope from the upper left field and then, in a "zigzag" fashion with equidistant movement. G-ratio was measured as inner/outer diameter of the myelin sheath (300 axons per animal).

MiRNA in situ hybridization

In situ hybridization (ISH) for miR-223 and miR-146 (miRCURY LNA miRNA probes, Exiqon) was performed using miRCURY LNA microRNA ISH Kit (Exiqon) according to manufacturer's protocol. In brief, cryosections were air dried at room temperature and treated with Proteinase-K for 10 min, washed twice in PBS. Hybridization mix was then applied for 60 min at 52°C following washes in descending concentrations of SSC buffers. Next, sections were incubated sequentially in blocking solution for 15 min and anti-DIG reagent conjugated with rhodamine (Roche) for 60 min. After three washes with PBS and counterstained with DAPI, slides were mounted with Floro-Gel Mounting Media (EMS) and imaged with ZEISS AX10 fluorescence microscope.

Supplementary Figure legends

Supplementary Fig. 1. Spinal cord-derived mGRPs express macroglial lineage but not neuronal markers. PLP-GFP-positive mGRP cells were isolated from E13.5 mouse spinal cord

and cultured in selection medium for 10 days. Immunocytochemistry was performed against multiple marker antigens indicated at the upper right corners of each images. Scale bar: 50 μm.

Supplementary Fig. 2. Immunocytochemistry for migration-mediating molecules. PLP-GFP-positive mGRP cells were isolated from E13.5 mouse spinal cord and cultured in selection medium for 10 days. Immunocytochemistry was performed with (**A**) CXCR4 and (**B**) FGFR antibodies. Scale bar: 50 μm.

Supplementary Fig. 3. Additional CTLA4-Ig application does not further enhance graft survival. Logarithmic BLI values of non-booster group (MR-1 and CTLA4-Ig treatment on POD0, 2, 4, 6, n=5), booster group (additional CTLA4-Ig application on POD30, 60, 90, n=5), and control group of B6 mice (n=5) that received intracerebral mGRP transplantation. There was no statistical difference between booster and non-booster group at any time-point examined. Both booster (*, $p<0.05$) and non-booster group BLI signals ($^{\#}$, $p<0.05$) were significantly higher than in the control group from POD14 onwards. Regression analysis was reported as type III tests of fixed effects, with the lowest mean square (LMS) difference test used for comparison between means (PROC MIXED, SAS 9.2). A coefficient of determination was calculated, and the BLI data were subjected to logistic transformation to maximize the model fit.

Supplementary Fig. 4. Costimulation blockade protects xenogeneic GRPs from immune rejection. Intracerebral hGRP engrafted B6 mice were subjected to longitudinal BLI and the logarithmic total flux over their heads were plotted. The statistically significant difference between

CoB and control group (*, $p<0.05$, n=5) started from POD9 and lasted till POD19. There were no BLI signal differences between CoB and scid groups ($p>0.4$, n=5). Regression analysis was reported as type III tests of fixed effects, with the lowest mean square (LMS) difference test used for comparison between means (PROC MIXED, SAS 9.2). A coefficient of determination was calculated, and the BLI data were subjected to logistic transformation to maximize the model fit. (**B**) Immunohistochemistry on B6 and scid mouse brain specimens was performed with STEM121 antibodies and DAPI staining on POD19. Scale bar: 100/10 μm in low/high magnificent images.

Supplementary Fig. 5. GRPs are vital after 19 days of intracerebral transplantation with costimulation blockade treatment. Confocal microscopy for PLP-GFP-positive mGRPs being transplanted into CoB, scid and control mouse brains on POD19. Cell nuclei were stained with DAPI. Note that mGRPs extended complex processes in CoB and scid brains indicating the integration into host brains, but displayed moribund morphology in control brains. Scale bar: 10 μm.

Supplementary Fig. 6. Peripheral Treg population is decreased in costimulation blockade treated mice. T cells isolated from naïve, control and CoB B6 mouse spleens were analyzed for the proportion (**A**) and absolute number (**B**) of $CD4^+$, $FoxP3^+$ Tregs by flow cytometry. Control mice had significantly more Tregs residing in the spleen than CoB mice on both POD5 ($p<0.0001$) and POD12 ($p=0.0016$). There was no difference in neither $CD4^+$ cell proportion (**C**) nor absolute numbers (**D**). Independent two sample *t*-test (SPSS 22.0).

Supplementary Fig. 7. Costimulation blockade mitigates the post-transplantation pro-inflammatory cytokine profile. Sera from intracerebrally mGRP transplanted CoB, control, and scid mice were drawn on POD5, 11, 17, 25 and subjected to a high throughput cytokine analysis. Cytokines that were within the detection range are presented with absolute values and standard deviation at different time-points examined. One-way ANOVA with LSD *post hoc* corrections. *$p<0.05$ between CoB and control mice, $^{\&}p<0.05$ between CoB and scid mice, $^{\#}p<0.05$ between scid and control mice (n=5 in each group).

Supplementary Fig. 8. Clustered heatmaps of the serum cytokines after intracerebral mGRP transplantation. Sera from intracerebral mGRP transplanted CoB, control, and scid mice were drawn on POD5, 11, 17, 25 and subjected to a high throughput cytokine analysis. Cluster analysis was performed with NCSS Statistical Software based on the quantitative data presented in Supplementary Fig. 7.

Supplementary Fig. 9. Costimulation blockade upregulates intragraft miR-146 expression post mGRP transplantation. *In situ* miRNA hybridization with DAPI counterstaining was performed for mGRP transplanted CoB and control mouse brains on POD19. (**A**) Mouse brain cryosections were hybridized with miR-146 probes and note its increased expression co-localizing with mGRPs in CoB brains. Control brains were negative for miR-146 hybridization. (**B**). Mouse brain cryosections were hybridized with miR-223 probes. There was no positive hybridization in neither CoB nor control brains. Scale bar: 50 μm.

Supplementary Table 1. GFP-MBP co-localization parameters.

References

Adams AB, Ford ML, Larsen CP. Costimulation Blockade in Autoimmunity and Transplantation: The CD28 Pathway. J Immunol 2016; 197(6): 2045-50.

Anglicheau D, Sharma VK, Ding R, Hummel A, Snopkowski C, Dadhania D, et al. MicroRNA expression profiles predictive of human renal allograft status. Proc Natl Acad Sci U S A 2009; 106(13): 5330-5.

Berman SC, Galpoththawela C, Gilad AA, Bulte JW, Walczak P. Long-term MR cell tracking of neural stem cells grafted in immunocompetent versus immunodeficient mice reveals distinct differences in contrast between live and dead cells. Magn Reson Med 2011; 65(2): 564-74.

Betts G, Shankar S, Sherston S, Friend P, Wood KJ. Examination of serum miRNA levels in kidney transplant recipients with acute rejection. Transplantation 2014; 97(4): e28-30.

Biname F, Sakry D, Dimou L, Jolivel V, Trotter J. NG2 regulates directional migration of oligodendrocyte precursor cells via Rho GTPases and polarity complex proteins. J Neurosci 2013; 33(26): 10858-74.

Bluestone JA, St Clair EW, Turka LA. CTLA4Ig: bridging the basic immunology with clinical application. Immunity 2006; 24(3): 233-8.

Bohmig GA, Wahrmann M, Saemann MD. Detecting adaptive immunity: applications in transplantation monitoring. Mol Diagn Ther 2010; 14(1): 1-11.

Boltze J, Nitzsche F, Jolkkonen J, Weise G, Posel C, Nitzsche B, et al. Concise Review: Increasing the Validity of Cerebrovascular Disease Models and Experimental Methods for Translational Stem Cell Research. Stem Cells 2017; 35(5): 1141-53.

Bribian A, Barallobre MJ, Soussi-Yanicostas N, de Castro F. Anosmin-1 modulates the FGF-2-dependent migration of oligodendrocyte precursors in the developing optic nerve. Mol Cell Neurosci 2006; 33(1): 2-14.

Camirand G, Riella LV. Treg-Centric View of Immunosuppressive Drugs in Transplantation: A Balancing Act. Am J Transplant 2017; 17(3): 601-10.

Chavez H, Beaudreuil S, Abbed K, Taoufic Y, Kriaa F, Charpentier B, et al. Absence of CD4CD25 regulatory T cell expansion in renal transplanted patients treated in vivo with Belatacept mediated CD28-CD80/86 blockade. Transpl Immunol 2007; 17(4): 243-8.

Diehl R, Ferrara F, Muller C, Dreyer AY, McLeod DD, Fricke S, et al. Immunosuppression for in vivo research: state-of-the-art protocols and experimental approaches. Cell Mol Immunol 2017; 14(2): 146-79.

Ehrlich M, Mozafari S, Glatza M, Starost L, Velychko S, Hallmann AL, et al. Rapid and efficient generation of oligodendrocytes from human induced pluripotent stem cells using transcription factors. Proc Natl Acad Sci U S A 2017; 114(11): E2243-E52.

Gansmuller A, Lachapelle F, Baron-Van Evercooren A, Hauw JJ, Baumann N, Gumpel M. Transplantations of newborn CNS fragments into the brain of shiverer mutant mice: extensive myelination by transplanted oligodendrocytes. II. Electron microscopic study. Dev Neurosci 1986; 8(4): 197-207.

Gaudet AD, Fonken LK, Watkins LR, Nelson RJ, Popovich PG. MicroRNAs: Roles in Regulating Neuroinflammation. Neuroscientist 2017: 1073858417721150.

Gilson CR, Milas Z, Gangappa S, Hollenbaugh D, Pearson TC, Ford ML, et al. Anti-CD40 monoclonal antibody synergizes with CTLA4-Ig in promoting long-term graft survival in murine models of transplantation. J Immunol 2009; 183(3): 1625-35.

Goldman SA. Stem and Progenitor Cell-Based Therapy of the Central Nervous System: Hopes, Hype, and Wishful Thinking. Cell Stem Cell 2016; 18(2): 174-88.

Goldman SA, Nedergaard M, Windrem MS. Glial progenitor cell-based treatment and modeling of neurological disease. Science 2012; 338(6106): 491-5.

Graves SS, Stone D, Loretz C, Peterson L, McCune JS, Mielcarek M, et al. Establishment of long-term tolerance to SRBC in dogs by recombinant canine CTLA4-Ig. Transplantation 2009; 88(3): 317-22.

Haas C, Fischer I. Human astrocytes derived from glial restricted progenitors support regeneration of the injured spinal cord. J Neurotrauma 2013; 30(12): 1035-52.

Hamdorf M, Kawakita S, Everly M. The Potential of MicroRNAs as Novel Biomarkers for Transplant Rejection. J Immunol Res 2017; 2017: 4072364.

Harlow DE, Saul KE, Culp CM, Vesely EM, Macklin WB. Expression of proteolipid protein gene in spinal cord stem cells and early oligodendrocyte progenitor cells is dispensable for normal cell migration and myelination. J Neurosci 2014; 34(4): 1333-43.

Harlow DE, Saul KE, Komuro H, Macklin WB. Myelin Proteolipid Protein Complexes with alphav Integrin and AMPA Receptors In Vivo and Regulates AMPA-Dependent Oligodendrocyte Progenitor Cell Migration through the Modulation of Cell-Surface GluR2 Expression. J Neurosci 2015; 35(34): 12018-32.

Hoefig KP, Heissmeyer V. MicroRNAs grow up in the immune system. Curr Opin Immunol 2008; 20(3): 281-7.

Hu J, Wang Z, Tan CJ, Liao BY, Zhang X, Xu M, et al. Plasma microRNA, a potential biomarker for acute rejection after liver transplantation. Transplantation 2013; 95(8): 991-9.

Janowski M, Engels C, Gorelik M, Lyczek A, Bernard S, Bulte JW, et al. Survival of neural progenitors allografted into the CNS of immunocompetent recipients is highly dependent on transplantation site. Cell Transplant 2014; 23(2): 253-62.

Janowski M, Lyczek A, Engels C, Xu J, Lukomska B, Bulte JW, et al. Cell size and velocity of injection are major determinants of the safety of intracarotid stem cell transplantation. J Cereb Blood Flow Metab 2013; 33(6): 921-7.

Kinnear G, Jones ND, Wood KJ. Costimulation blockade: current perspectives and implications for therapy. Transplantation 2013; 95(4): 527-35.

Kirk AD, Guasch A, Xu H, Cheeseman J, Mead SI, Ghali A, et al. Renal transplantation using belatacept without maintenance steroids or calcineurin inhibitors. Am J Transplant 2014; 14(5): 1142-51.

Kishimoto K, Dong VM, Issazadeh S, Fedoseyeva EV, Waaga AM, Yamada A, et al. The role of CD154-CD40 versus CD28-B7 costimulatory pathways in regulating allogeneic Th1 and Th2 responses in vivo. J Clin Invest 2000; 106(1): 63-72.

Lachapelle F, Gumpel M, Baulac M, Jacque C, Duc P, Baumann N. Transplantation of CNS fragments into the brain of shiverer mutant mice: extensive myelination by implanted oligodendrocytes. I. Immunohistochemical studies. Dev Neurosci 1983; 6(6): 325-34.

Lafferty KJ, Prowse SJ, Simeonovic CJ, Warren HS. Immunobiology of tissue transplantation: a return to the passenger leukocyte concept. Annu Rev Immunol 1983; 1: 143-73.

Larsen CP, Elwood ET, Alexander DZ, Ritchie SC, Hendrix R, Tucker-Burden C, et al. Long-term acceptance of skin and cardiac allografts after blocking CD40 and CD28 pathways. Nature 1996; 381(6581): 434-8.

Lenschow DJ, Zeng Y, Thistlethwaite JR, Montag A, Brady W, Gibson MG, et al. Long-term survival of xenogeneic pancreatic islet grafts induced by CTLA4lg. Science 1992; 257(5071): 789-92.

Lepore AC, Walczak P, Rao MS, Fischer I, Bulte JW. MR imaging of lineage-restricted neural precursors following transplantation into the adult spinal cord. Exp Neurol 2006; 201(1): 49-59.

Levitsky J, Miller J, Huang X, Chandrasekaran D, Chen L, Mathew JM. Inhibitory effects of belatacept on allospecific regulatory T-cell generation in humans. Transplantation 2013; 96(8): 689-96.

Lin H, Wei RQ, Goodman RE, Bolling SF. CD28 blockade alters cytokine mRNA profiles in cardiac transplantation. Surgery 1997; 122(2): 129-37.

Lyczek A, Arnold A, Zhang J, Campanelli JT, Janowski M, Bulte JW, et al. Transplanted human glial-restricted progenitors can rescue the survival of dysmyelinated mice independent of the production of mature, compact myelin. Exp Neurol 2017; 291: 74-86.

Marino J, Paster J, Benichou G. Allorecognition by T Lymphocytes and Allograft Rejection. Front Immunol 2016; 7: 582.

Masson P, Henderson L, Chapman JR, Craig JC, Webster AC. Belatacept for kidney transplant recipients. Cochrane Database Syst Rev 2014(11): CD010699.

Mehta A, Baltimore D. MicroRNAs as regulatory elements in immune system logic. Nat Rev Immunol 2016; 16(5): 279-94.

Morita M, Chen J, Fujino M, Kitazawa Y, Sugioka A, Zhong L, et al. Identification of microRNAs involved in acute rejection and spontaneous tolerance in murine hepatic allografts. Sci Rep 2014; 4: 6649.

Oh AL, Mahmud D, Nicolini B, Mahmud N, Senyuk V, Patel PR, et al. T Cell-Mediated Rejection of Human CD34+ Cells Is Prevented by Costimulatory Blockade in a Xenograft Model. Biol Blood Marrow Transplant 2017.

Pearl JI, Lee AS, Leveson-Gower DB, Sun N, Ghosh Z, Lan F, et al. Short-term immunosuppression promotes engraftment of embryonic and induced pluripotent stem cells. Cell Stem Cell 2011; 8(3): 309-17.

Phillips AW, Falahati S, DeSilva R, Shats I, Marx J, Arauz E, et al. Derivation of glial restricted precursors from E13 mice. J Vis Exp 2012(64).

Piao J, Major T, Auyeung G, Policarpio E, Menon J, Droms L, et al. Human embryonic stem cell-derived oligodendrocyte progenitors remyelinate the brain and rescue behavioral deficits following radiation. Cell Stem Cell 2015; 16(2): 198-210.

Rao MS, Mayer-Proschel M. Glial-restricted precursors are derived from multipotent neuroepithelial stem cells. Dev Biol 1997; 188(1): 48-63.

Rao MS, Noble M, Mayer-Proschel M. A tripotential glial precursor cell is present in the developing spinal cord. Proc Natl Acad Sci U S A 1998; 95(7): 3996-4001.

Sajja V, Jablonska A, Haughey NJ, Bulte JWM, Stevens RD, Long J, et al. Neurolipids and microRNA changes in blood following blast traumatic brain injury in mice: an exploratory study. J Neurotrauma 2017.

Sandrock RW, Wheatley W, Levinthal C, Lawson J, Hashimoto B, Rao M, et al. Isolation, characterization and preclinical development of human glial-restricted progenitor cells for treatment of neurological disorders. Regen Med 2010; 5(3): 381-94.

Schjenken JE, Zhang B, Chan HY, Sharkey DJ, Fullston T, Robertson SA. miRNA Regulation of Immune Tolerance in Early Pregnancy. Am J Reprod Immunol 2016; 75(3): 272-80.

Semenkow S, Li S, Kahlert UD, Raabe EH, Xu J, Arnold A, et al. An immunocompetent mouse model of human glioblastoma. Oncotarget 2017.

Shiraishi T, Yasunami Y, Takehara M, Uede T, Kawahara K, Shirakusa T. Prevention of acute lung allograft rejection in rat by CTLA4Ig. Am J Transplant 2002; 2(3): 223-8.

Srivastava AK, Bulte CA, Shats I, Walczak P, Bulte JW. Co-transplantation of syngeneic mesenchymal stem cells improves survival of allogeneic glial-restricted precursors in mouse brain. Exp Neurol 2016; 275 Pt 1: 154-61.

Sui W, Dai Y, Huang Y, Lan H, Yan Q, Huang H. Microarray analysis of MicroRNA expression in acute rejection after renal transplantation. Transpl Immunol 2008; 19(1): 81-5.

Szot GL, Yadav M, Lang J, Kroon E, Kerr J, Kadoya K, et al. Tolerance induction and reversal of diabetes in mice transplanted with human embryonic stem cell-derived pancreatic endoderm. Cell Stem Cell 2015; 16(2): 148-57.

Tsai HH, Niu J, Munji R, Davalos D, Chang J, Zhang H, et al. Oligodendrocyte precursors migrate along vasculature in the developing nervous system. Science 2016; 351(6271): 379-84.

Verbinnen B, Van Gool SW, Ceuppens JL. Blocking costimulatory pathways: prospects for inducing transplantation tolerance. Immunotherapy 2010; 2(4): 497-509.

Walczak P, All AH, Rumpal N, Gorelik M, Kim H, Maybhate A, et al. Human glial-restricted progenitors survive, proliferate, and preserve electrophysiological function in rats with focal inflammatory spinal cord demyelination. Glia 2011; 59(3): 499-510.

Wang S, Bates J, Li X, Schanz S, Chandler-Militello D, Levine C, et al. Human iPSC-derived oligodendrocyte progenitor cells can myelinate and rescue a mouse model of congenital hypomyelination. Cell Stem Cell 2013; 12(2): 252-64.

Webber AB, Vincenti F. An Update on Calcineurin Inhibitor-Free Regimens: The Need Persists, but the Landscape has Changed. Transplantation 2016; 100(4): 836-43.

Windrem MS, Nunes MC, Rashbaum WK, Schwartz TH, Goodman RA, McKhann G, 2nd, et al. Fetal and adult human oligodendrocyte progenitor cell isolates myelinate the congenitally dysmyelinated brain. Nat Med 2004; 10(1): 93-7.

Windrem MS, Schanz SJ, Guo M, Tian GF, Washco V, Stanwood N, et al. Neonatal chimerization with human glial progenitor cells can both remyelinate and rescue the otherwise lethally hypomyelinated shiverer mouse. Cell Stem Cell 2008; 2(6): 553-65.

Table 1. Animal assignment and measurements.

Animal number			Endpoint (day)	Measurements
B6 CoB	B6 control	scid		
5[A] + 5[B]	5[C]	5[D]	203	• mGRP allograft survival (BLI) •secondary mGRP allograft survival (BLI) •adoptive transfer •immunohistochemistry •cytokine analysis
5	5	5	19	•IHC
5	5		5	•miRNA analysis, Treg analysis
5	5		12	•miRNA analysis, Treg analysis
10[E]	10[E]		19	•miRNA analysis
5	5	5	19	•hGRP xenograft survival (BLI)
Shiverer -CoB	Shiverer -control	Shiverer -rag2		
5	5	5	33	•BLI, MLR, IHC, Erichrome staining
5	5	5	90	•BLI, MRI, Erichrome staining, IHC, EM

[A]non-booster: CTLA4-Ig+MR-1 on POD0, 2, 4, 6. One sacrificed (on POD154). [B]booster: CTLA4-Ig+MR-1 on POD0, 2, 4, 6 and monthly CTLA4-Ig. One died (POD50). [C]: One died (POD57. One sacrificed (POD154). [D]: One died (POD28). One died (POD126). [E]: Five with mGRP transplantation.

Figure legends

Fig. 1. Costimulation blockade induces long-term engraftment of allogeneic GRPs. B6 and scid mice were recipients for luciferase-expressing mGRPs. (**A**) Logarithmic BLI total flux over the mouse heads was plotted longitudinally for 203 days. Statistically significant difference between CoB and control group (*, $p<0.05$, n=5), and scid and control group ($^{\#}$, $p<0.05$, n=5) started from POD14. (**B**) On POD120, three CoB and three scid mice received a second, subcutaneous mGRP transplantation to their back. Five naïve B6 mice served as controls. BLI values were plotted and the statistical difference between CoB and control group started from POD17 (*, $p<0.05$). (**C**) BLI image of mice that received both intracerebral and subcutaneous transplantation of mGRPs (POD203 of intracerebral transplantation). BLI intensity scale is shown on the right. (**D**) T cells isolated from one naïve B6 mouse, one CoB, and one control mouse on POD154 were retro-orbitally injected into scid mice with five different combinations (n=4). Four days after T cell inoculation, these scid mice received subcutaneous mGRP injection into their back and subsequent serial BLI. BLI signals were significantly different between CoB and control group on POD7 ($p<0.0001$). Regression analysis was reported as type III tests of fixed effects, with the lowest mean square (LMS) difference test used for comparison between means (PROC MIXED, SAS 9.2). A coefficient of determination was calculated, and the BLI data were subjected to logistic transformation to maximize the model fit. (**E**) Immunohistochemistry with anti-CD45 antibodies (leukocytes) and DAPI for CoB, control and scid mouse brains on POD154. Note the absence of CD45-positive cells in CoB brain. Scale bar: 50 μm.

Fig. 2. T cell recruitment elicited to GRP allografts is abrogated by costimulation blockade. (**A**) CD45 immunostaining was performed for B6 and scid mouse brains on POD19. Scale bar:

100/20 μm in low/high magnificent images. (**B**) Schematic diagram showing the area of mGRP engraftment and immune cell infiltration assessment outlined with a red line and covered by a 0.05 X 0.1 cm rectangle (grey). The red fluorescence intensity in the transplanted side was measured and normalized to a corresponding area at the contralateral side (second rectangle) of each mouse. (**C**) Statistical difference was revealed between CoB and control group in CD45-positive areas (*, p=0.011), but not between CoB and scid group (p=1.000), n=5. (**D**) A statistically significant difference was revealed between CoB and control group in CD45 intensity (*, p=0.001), but not between CoB and scid group (p=0.231), n=5. Independent samples Kruskal-Wallis (2-sided) test with Bonferroni's adjustment (SPSS 22.0). (**E**) Immunohistochemistry was performed for B6 and scid mouse brains with CD3 antibodies and DAPI staining on POD19. T cells were robustly recruited around the mGRP allografts in the control group but were absent in CoB and scid groups. Scale bar: 50/10 μm in low/high magnificent images. (**F**) Counting of CD3-positive cells in the total brain slices showed that statistically less T cells were recruited to both CoB brains and scid brains as compared to control brains (scid versus control, p=0.042, CoB versus control, *, p=0.046) and there was no difference between CoB group and scid group (p=1.000), n=5. One way ANOVA with Bonferroni's adjustment (SPSS 22.0).

Fig. 3. Phagocytic activity against allografts is prohibited by costimulation blockade. (**A**) Iba-1 immunostaining was performed for B6 and scid mouse brains on POD19. Scale bar: 50 μm. (**B**) There was no statistical difference between any two groups in Ibal-1 intensity, n=5. (**C**) Statistical difference was revealed between CoB and control group for Iba-1-positive areas (*, p=0.033, n=5), but not between CoB and scid group (p=1.000), n=5. (**D**) CD68 immunostaining was performed for B6 and scid mouse brains on POD19. Scale bar: 50 μm. (**E**) There was statistical difference in CD68 intensity between CoB and control group (*, p=0.021), scid and control group (p=0.026),

but not between CoB and control group (p=1.000), n=5. (**F**) Statistical difference was revealed between CoB and control group for CD68-positive area (*, p=0.003, n=5), but not between CoB and scid group (p=1.000), n=5. Independent samples Kruskal-Wallis (2-sided) test with Bonferroni's adjustment (SPSS 22.0).

Fig. 4. Costimulation blockade induces long-term survival of GRPs in dysmyelinated shiverer mice. (**A**) MGRP engrafted shiverer mice were subjected to longitudinal BLI and the logarithmic total flux were plotted. The statistically significant difference between shiverer-CoB and shiverer-control groups (*, $p<0.05$, n=5) as well as shiverer-rag2 and shiverer-control groups ($^{\#}$, $p<0.05$, n=5) started from POD14 and lasted until POD90. There were no BLI signal differences between shiverer-CoB and shiverer-rag2 groups ($p>0.4$, n=5). Regression analysis was reported as type III tests of fixed effects, with the lowest mean square (LMS) difference test used for comparison between means (PROC MIXED, SAS 9.2). A coefficient of determination was calculated, and the BLI data were subjected to logistic transformation to maximize the model fit. (**B**) BLI image of mGRP-transplanted shiverer mice (POD90). (**C**-**D**) T cells isolated from shiverer-CoB or shiverer-control mice were co-cultured with either intact or minced mGRPs in the presence of either APCs or third party APCs. The proliferation of $CD4^+$ T cells (C) and $CD8^+$ T cells (D) were analyzed by flow cytometry and normalized to age-matched naïve shiverer mouse levels. There was a statistically significant difference between control and CoB group when cultured with donor-matched APC in presence of minced mGRP ($CD4^+$, *, p=0.0277, n=3, $CD8^+$, *, p=0.0364, n=3), and when cultured with third party-derived APC in presence of intact mGRP ($CD4^+$, *, p=0.0206, n=3, $CD8^+$, p=0.0277, n=3). Independent two sample *t*-test (SPSS 22.0).

Fig. 5. GRPs engrafted into shiverer mouse brains differentiate into MBP-positive oligodendrocytes. (**A**) T2-weighted image of a 4-month old rag2-/- (rag2) mouse. Scale bar: 5 mm. (**B**) MGRP-transplanted shiverer mice were subjected to T2-weighted MRI. Note the hypointensity in shiverer-rag2 and shiverer-CoB brains along the corpus callosum (white arrows) on POD90. (**C**) Immunohistochemistry was performed using MBP antibodies and DAPI for mGRP-transplanted shiverer mouse brains on POD33 and POD90 (corresponding to the mice imaged in (B)). Note that the MBP-positive region co-localized with the engrafted GFP-expressing mGRPs. There was neither green nor red fluorescence in shiverer-control mice on POD90. Scale bar: 200 μm. (**D**) Confocal microscopy of POD90 mGRP engrafted shiverer brain to better appreciate the cell morphology and GFP-MBP co-localization. Scale bar: 10 μm.

Fig. 6. Protected by costimulation, allogeneic GRPs form myelin in dysmyelinated shiverer brains. (**A**) Erichrome cyanin staining was carried out for mGRP transplanted shiverer mouse brains on POD33, 73, and 90. Positive staining was observed along the corpus callosum on POD73 and POD90 in shiverer-rag2 and shiverer-CoB brains but was absent in shiverer-CoB brain on POD33 and shiverer-control brain on POD90. Scale bar: 500 μm. (**B**) Transmission electron microscopy with shiverer corpus callosum at Bregma level in the transplanted hemisphere on POD90. Upper images: mGRP transplanted shiverer-CoB. Lower images: mGRP transplanted shiverer-control. Left panel, lower magnification. Right panel, higher magnification. Scale bar: 500 nm. Side length of upper right insets: 300 nm.

Fig. 7. Dynamic changes of miRNA could serve as graft tolerance/rejection biomarkers. MiRNA was isolated from CoB and control B6 mouse plasma on POD2, 5, 12 and 19 of

intracerebral mGRP transplantation and the expression of miR-146, miR-223, let 7a/7c, miR-150, and miR-125b was measured and normalized to their pre-transplantation levels. One way ANOVA with Bonferroni's adjustment, *, $p<0.05$ between two adjacent time-points in GRPs+PBS or GRPs+CoB groups. #, GRPs+CoB vs. GRPs+PBS, &, GRPs+PBS vs. surgery+CoB, §, GRPs+PBS vs. surgery+PBS, $, GRPs+CoB vs. sugery+CoB, † GRPs+CoB vs. surgery+PBS, $p<0.05$ comparison between two groups at identical time-points (*t*-test).

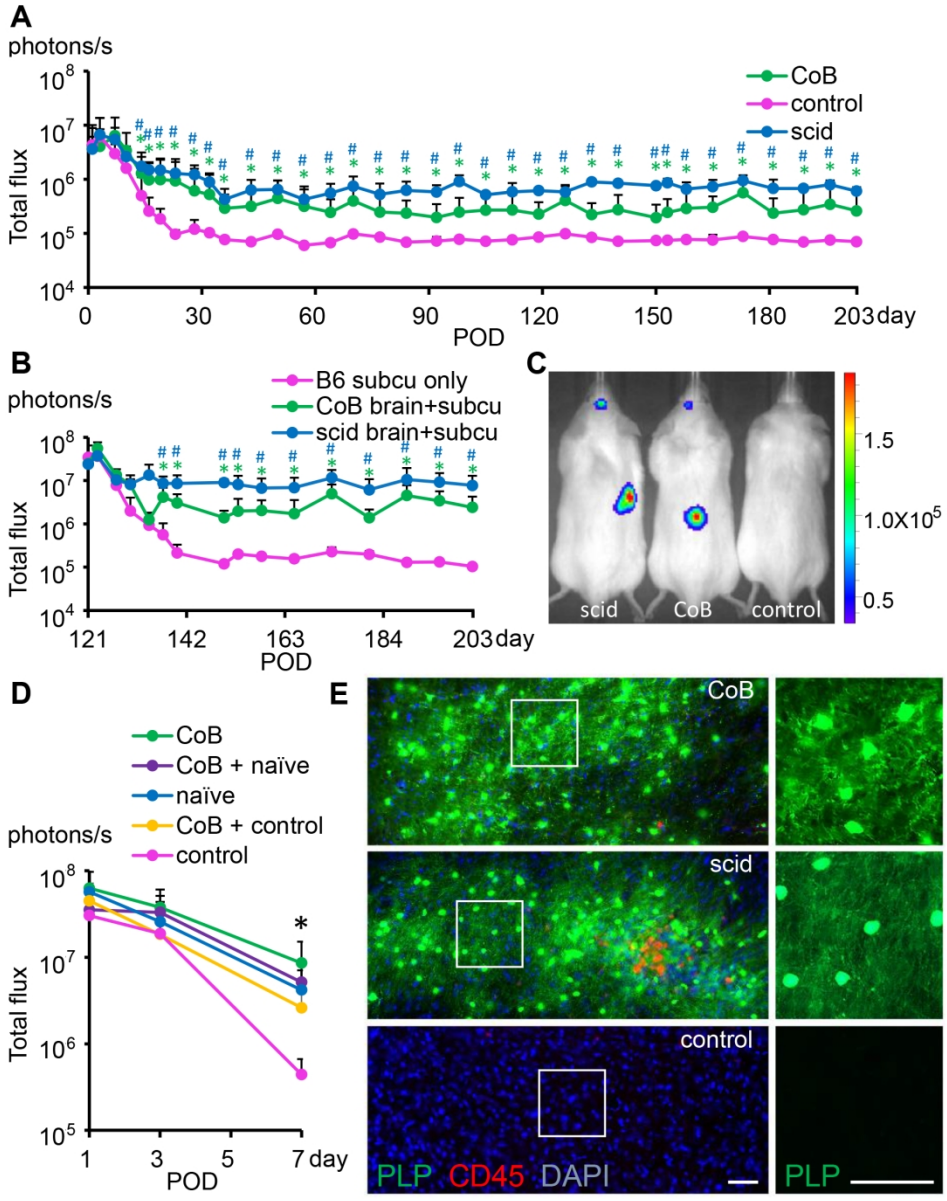

Fig. 1. Costimulation blockade induces long-term engraftment of allogeneic GRPs. B6 and scid mice were recipients for luciferase-expressing mGRPs. (A) Logarithmic BLI total flux over the mouse heads was plotted longitudinally for 203 days. Statistically significant difference between CoB and control group (*, $p<0.05$, $n=5$), and scid and control group (#, $p<0.05$, $n=5$) started from POD14. (B) On POD120, three CoB and three scid mice received a second, subcutaneous mGRP transplantation to their back. Five naïve B6 mice served as controls. BLI values were plotted and the statistical difference between CoB and control group started from POD17 (*, $p<0.05$). (C) BLI image of mice that received both intracerebral and subcutaneous transplantation of mGRPs (POD203 of intracerebral transplantation). BLI intensity scale is shown on the right. (D) T cells isolated from one naïve B6 mouse, one CoB, and one control mouse on POD154 were retro-orbitally injected into scid mice with five different combinations (n=4). Four days after T cell inoculation, these scid mice received subcutaneous mGRP injection into their back and subsequent serial BLI. BLI signals were significantly different between CoB and control group on POD7 ($p<0.0001$). Regression analysis was reported as type III tests of fixed effects, with the lowest mean square (LMS) difference test used for comparison between means (PROC MIXED, SAS 9.2). A coefficient of determination was calculated, and the

BLI data were subjected to logistic transformation to maximize the model fit. (E) Immunohistochemistry with anti-CD45 antibodies (leukocytes) and DAPI for CoB, control and scid mouse brains on POD154. Note the absence of CD45-positive cells in CoB brain. Scale bar: 50 μm.

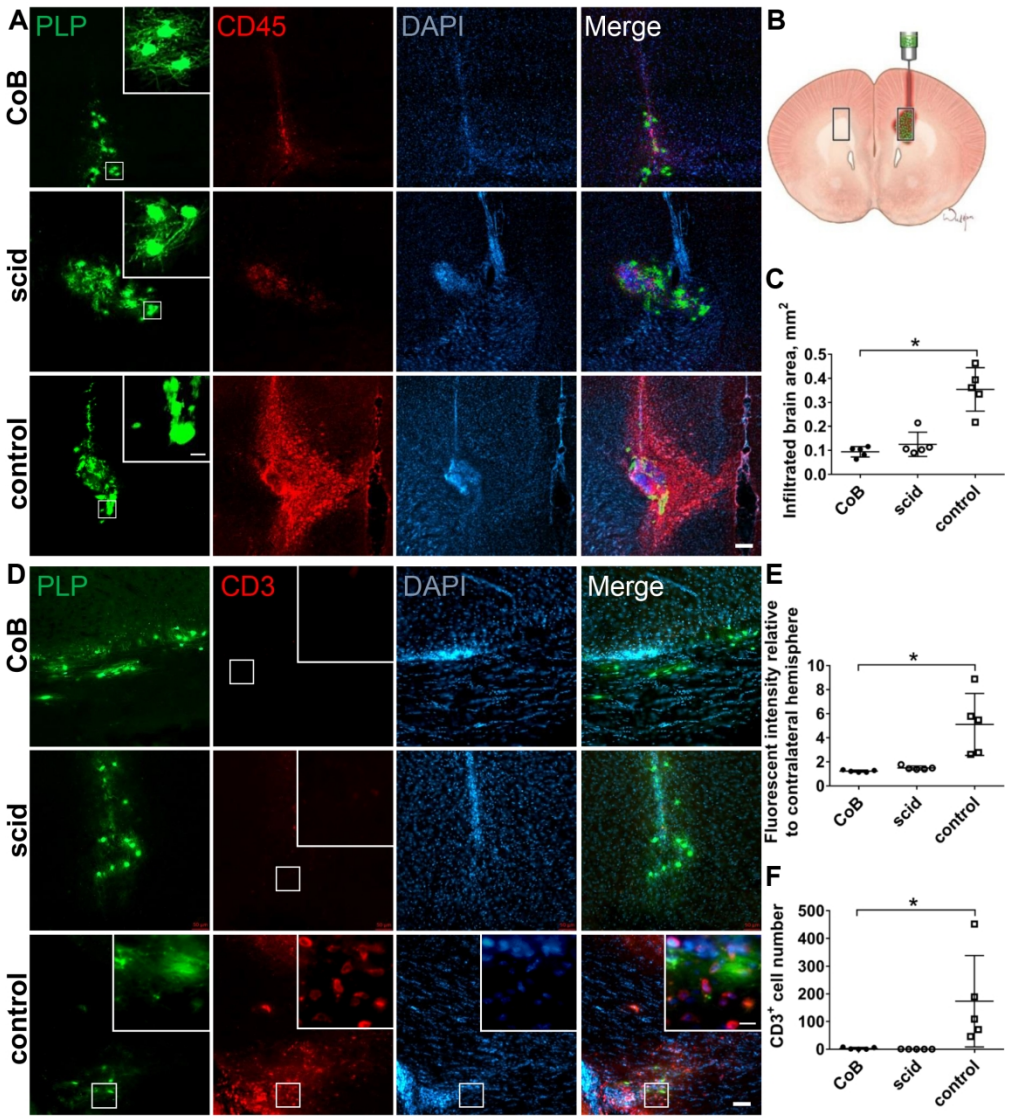

Fig. 2. T cell recruitment elicited to GRP allografts is abrogated by costimulation blockade. (A) CD45 immunostaining was performed for B6 and scid mouse brains on POD19. Scale bar: 100/20 μm in low/high magnificent images. (B) Schematic diagram showing the area of mGRP engraftment and immune cell infiltration assessment outlined with a red line and covered by a 0.05 X 0.1 cm rectangle (grey). The red fluorescence intensity in the transplanted side was measured and normalized to a corresponding area at the contralateral side (second rectangle) of each mouse. (C) Statistical difference was revealed between CoB and control group in CD45-positive areas (*, p=0.011), but not between CoB and scid group (p=1.000), n=5. (D) A statistically significant difference was revealed between CoB and control group in CD45 intensity (*, p=0.001), but not between CoB and scid group (p=0.231), n=5. Independent samples Kruskal-Wallis (2-sided) test with Bonferroni's adjustment (SPSS 22.0). (E) Immunohistochemistry was performed for B6 and scid mouse brains with CD3 antibodies and DAPI staining on POD19. T cells were robustly recruited around the mGRP allografts in the control group but were absent in CoB and scid groups. Scale bar: 50/10 μm in low/high magnificent images. (F) Counting of CD3-positive cells in the total brain slices showed that statistically less T cells were recruited to both CoB brains and scid brains as compared to control brains (scid versus control, p=0.042, CoB versus control, *, p=0.046) and there was no difference between CoB group and scid group (p=1.000), n=5. One way ANOVA with Bonferroni's adjustment (SPSS 22.0).

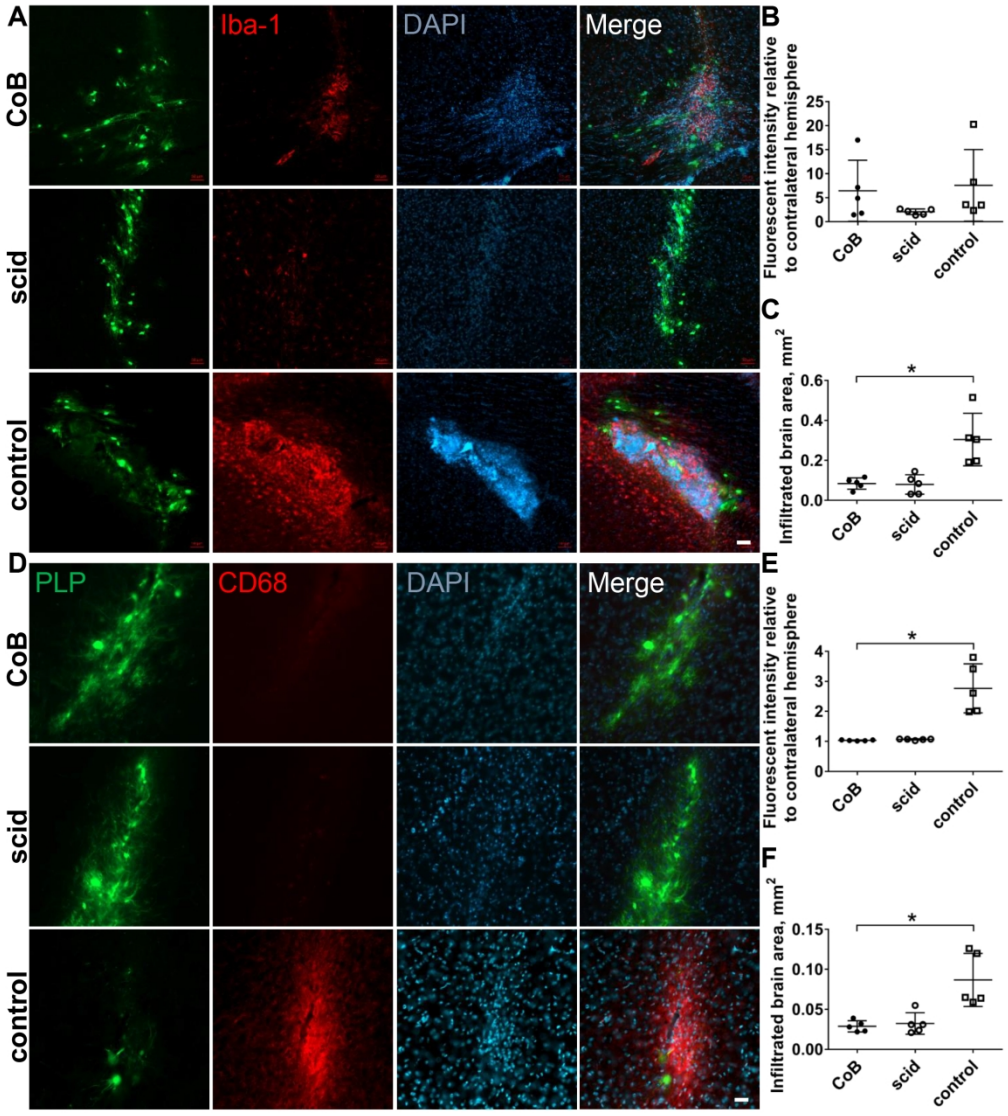

Fig. 3. Phagocytic activity against allografts is prohibited by costimulation blockade. (A) Iba-1 immunostaining was performed for B6 and scid mouse brains on POD19. Scale bar: 50 μm. (B) There was no statistical difference between any two groups in Ibal-1 intensity, n=5. (C) Statistical difference was revealed between CoB and control group for Iba-1-positive areas (*, p=0.033, n=5), but not between CoB and scid group (p=1.000), n=5. (D) CD68 immunostaining was performed for B6 and scid mouse brains on POD19. Scale bar: 50 μm. (E) There was statistical difference in CD68 intensity between CoB and control group (*, p=0.021), scid and control group (p=0.026), but not between CoB and control group (p=1.000), n=5. (F) Statistical difference was revealed between CoB and control group for CD68-positive area (*, p=0.003, n=5), but not between CoB and scid group (p=1.000), n=5. Independent samples Kruskal-Wallis (2-sided) test with Bonferroni's adjustment (SPSS 22.0).

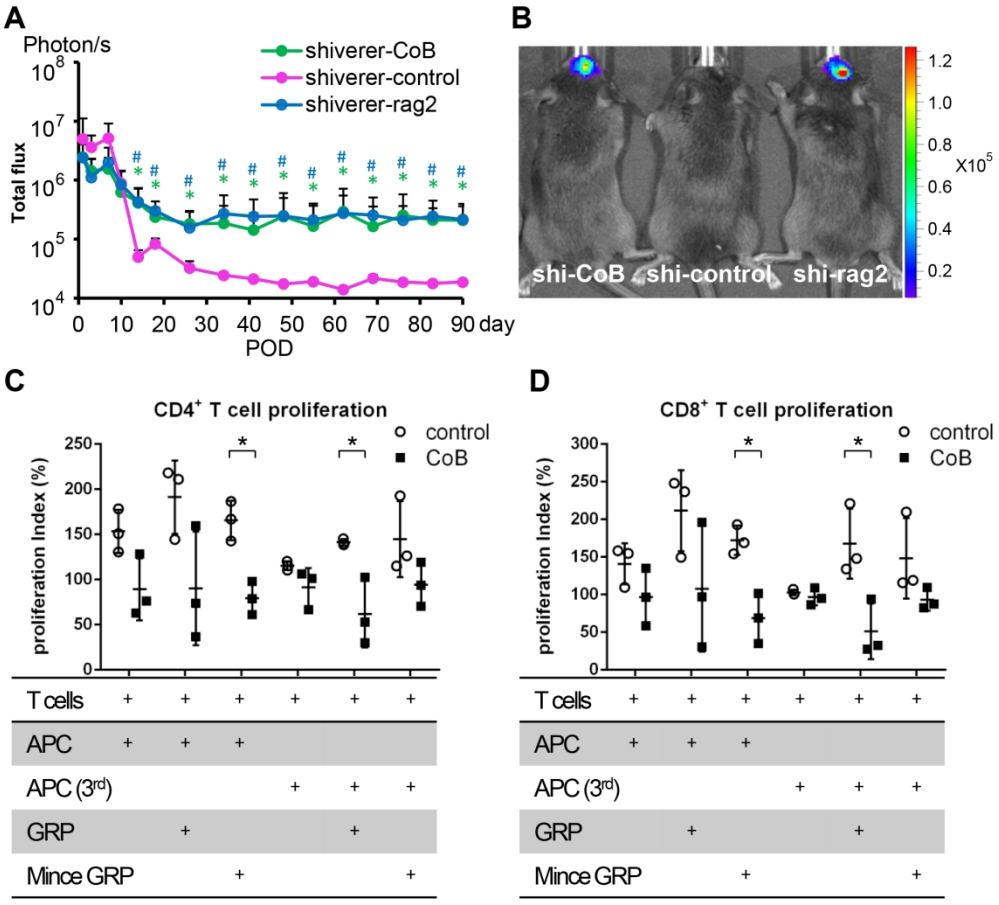

Fig. 4. Costimulation blockade induces long-term survival of GRPs in dysmyelinated shiverer mice. (A) MGRP engrafted shiverer mice were subjected to longitudinal BLI and the logarithmic total flux were plotted. The statistically significant difference between shiverer-CoB and shiverer-control groups (*, $p<0.05$, n=5) as well as shiverer-rag2 and shiverer-control groups (#, $p<0.05$, n=5) started from POD14 and lasted until POD90. There were no BLI signal differences between shiverer-CoB and shiverer-rag2 groups ($p>0.4$, n=5). Regression analysis was reported as type III tests of fixed effects, with the lowest mean square (LMS) difference test used for comparison between means (PROC MIXED, SAS 9.2). A coefficient of determination was calculated, and the BLI data were subjected to logistic transformation to maximize the model fit. (B) BLI image of mGRP-transplanted shiverer mice (POD90). (C-D) T cells isolated from shiverer-CoB or shiverer-control mice were co-cultured with either intact or minced mGRPs in the presence of either APCs or third party APCs. The proliferation of CD4+ T cells (C) and CD8+ T cells (D) were analyzed by flow cytometry and normalized to age-matched naïve shiverer mouse levels. There was a statistically significant difference between control and CoB group when cultured with donor-matched APC in presence of minced mGRP (CD4+, *, p=0.0277, n=3, CD8+, *, p=0.0364, n=3), and when cultured with third party-derived APC in presence of intact mGRP (CD4+, *, p=0.0206, n=3, CD8+, p=0.0277, n=3). Independent two sample t-test (SPSS 22.0).

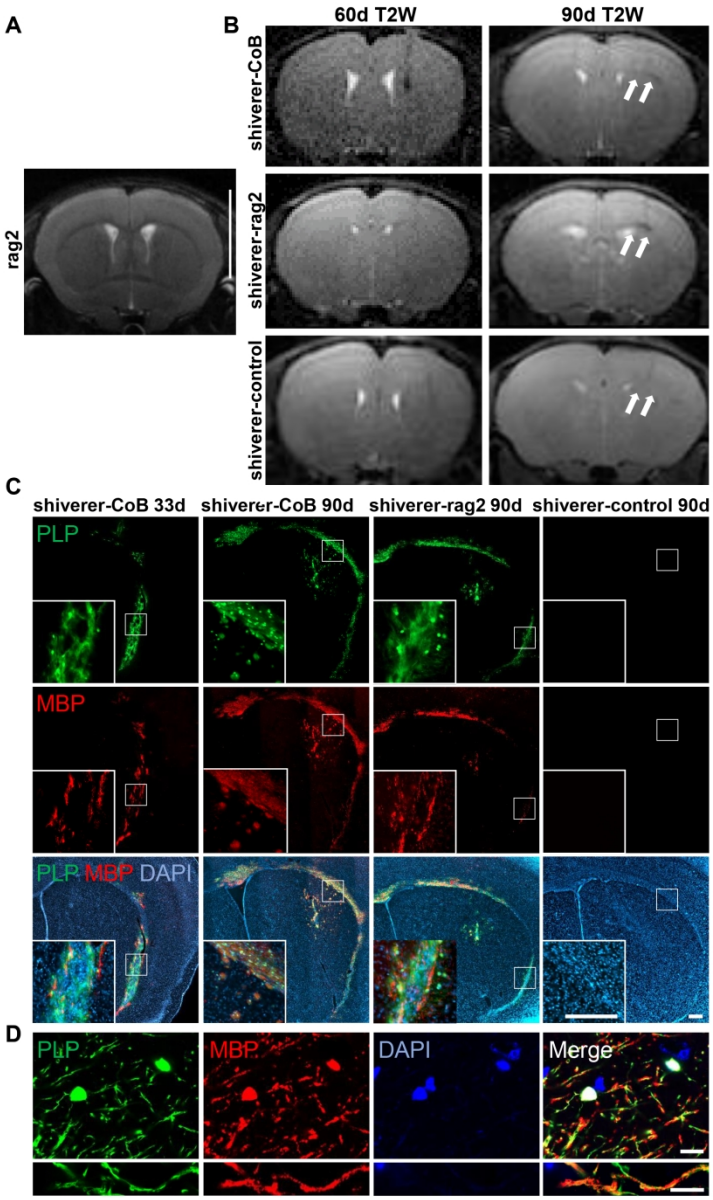

Fig. 5. GRPs engrafted into shiverer mouse brains differentiate into MBP-positive oligodendrocytes. (A) T2-weighted image of a 4-month old rag2-/- (rag2) mouse. Scale bar: 5 mm. (B) MGRP-transplanted shiverer mice were subjected to T2-weighted MRI. Note the hypointensity in shiverer-rag2 and shiverer-CoB brains along the corpus callosum (white arrows) on POD90. (C) Immunohistochemistry was performed using MBP antibodies and DAPI for mGRP-transplanted shiverer mouse brains on POD33 and POD90 (corresponding to the mice imaged in (B)). Note that the MBP-positive region co-localized with the engrafted GFP-expressing mGRPs. There was neither green nor red fluorescence in shiverer-control mice on POD90. Scale bar: 200 μm. (D) Confocal microscopy of POD90 mGRP engrafted shiverer brain to better appreciate the cell morphology and GFP-MBP co-localization. Scale bar: 10 μm.

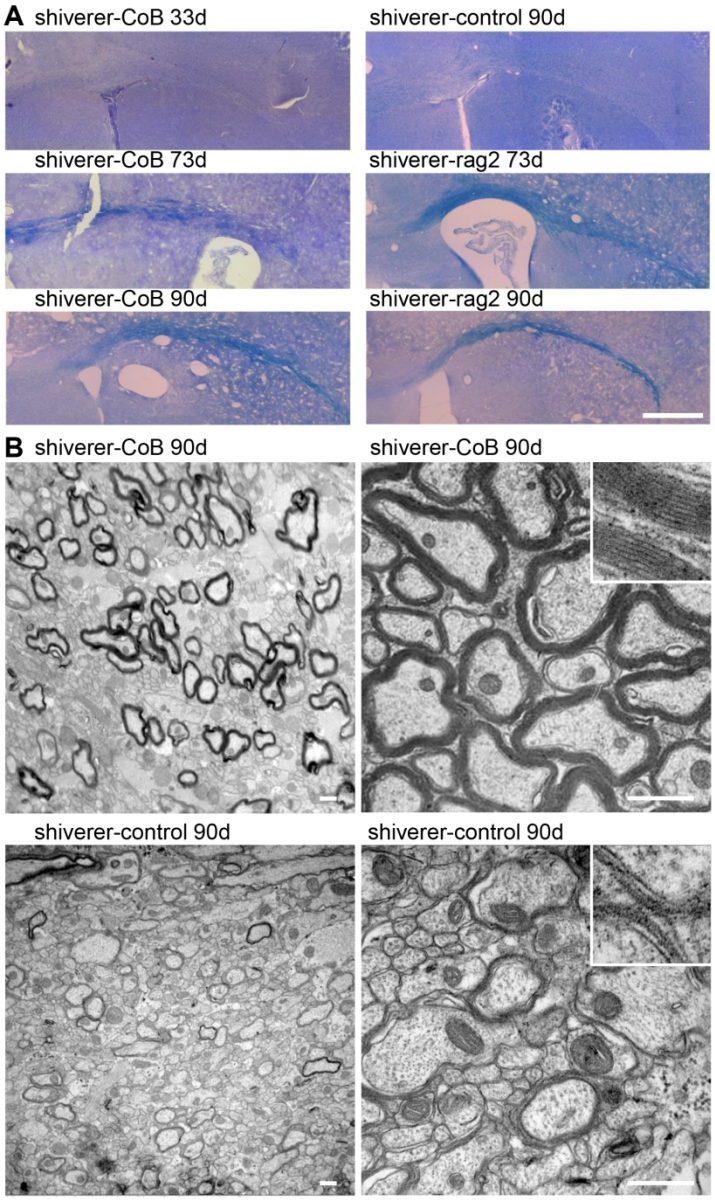

Fig. 6. Protected by costimulation, allogeneic GRPs form myelin in dysmyelinated shiverer brains. (A) Erichrome cyanin staining was carried out for mGRP transplanted shiverer mouse brains on POD33, 73, and 90. Positive staining was observed along the corpus callosum on POD73 and POD90 in shiverer-rag2 and shiverer-CoB brains but was absent in shiverer-CoB brain on POD33 and shiverer-control brain on POD90. Scale bar: 500 μm. (B) Transmission electron microscopy with shiverer corpus callosum at Bregma level in the transplanted hemisphere on POD90. Upper images: mGRP transplanted shiverer-CoB. Lower images: mGRP transplanted shiverer-control. Left panel, lower magnification. Right panel, higher magnification. Scale bar: 500 nm. Side length of upper right insets: 300 nm.

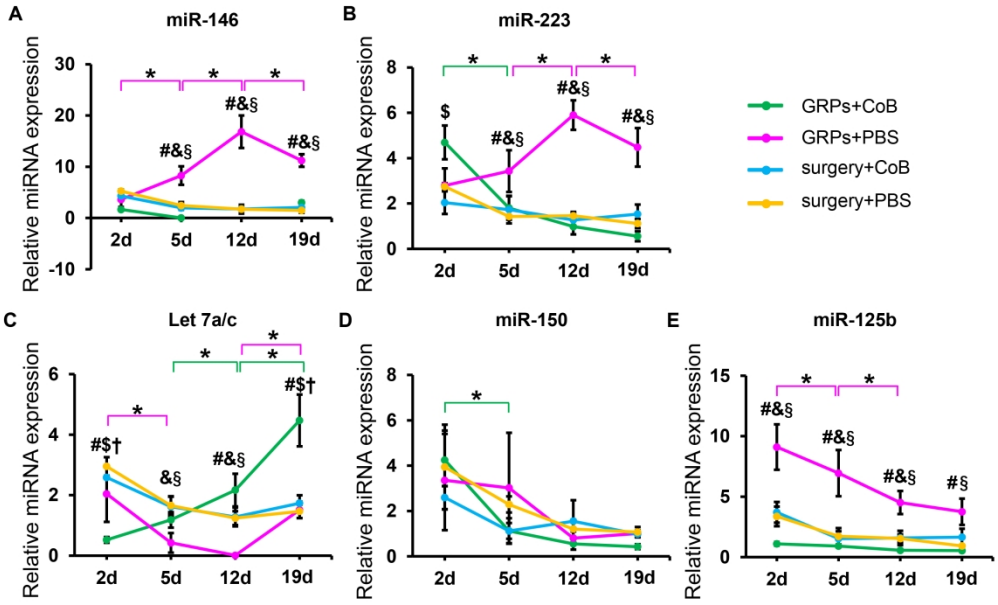

Fig. 7. Dynamic changes of miRNA could serve as graft tolerance/rejection biomarkers. MiRNA was isolated from CoB and control B6 mouse plasma on POD2, 5, 12 and 19 of intracerebral mGRP transplantation and the expression of miR-146, miR-223, let 7a/7c, miR-150, and miR-125b was measured and normalized to their pre-transplantation levels. One way ANOVA with Bonferroni's adjustment, *, $p<0.05$ between two adjacent time-points in GRPs+PBS or GRPs+CoB groups. #, GRPs+CoB vs. GRPs+PBS, &, GRPs+PBS vs. surgery+CoB, §, GRPs+PBS vs. surgery+PBS, $, GRPs+CoB vs. sugery+CoB, †GRPs+CoB vs. surgery+PBS, $p<0.05$ comparison between two groups at identical time-points (t-test).

Supplementary Materials

Supplementary Methods

Immunohistochemical analysis

Mice were anesthetized and perfused intracardially with 5% sucrose followed by PBS-buffered 4% paraformaldehyde. Brains were taken out, postfixed overnight at 4°C in 4% paraformaldehyde, dehydrated in 30% sucrose (Sigma-Aldrich), snap-frozen, and cryosectioned (Thermo Scientific HM 550 Cryostat) into 30-µm coronal sections. Nonspecific binding was blocked by incubating with 10% donkey serum in 0.1% Triton X-100-PBS for 1 h at room temperature. Appropriate dilutions of primary antibodies were then applied in blocking solution overnight at 4°C. After three washes, the corresponding secondary antibodies (in blocking solution, Alexa Fluro-594, Life Technologies-A11058) were incubated for 1 h at room temperature. Sections were then rinsed with PBS, counterstained with DAPI, and mounted with aqueous non-fluorescence mounting medium (Immu-mount, Thermo Scientific). Images were acquired with a Zeiss AX10 fluorescence microscope using the same exposure time and quantified with Image J. Primary antibodies were: anti-CD45 (1:500, Serotec-MCA1388); anti-Iba-1 (1:250, Wako-SAN3725); anti-CD3 (1:200, R&D-MAB4841); anti-CD68 (1:100, Abcam-ab31630); anti-MBP (1:1000, Serotec-MCA409S); anti-human cytoplasmic marker STEM121 (1:250, StemCells-AB-121-U050). The co-localization parameters between GFP and MBP was analyzed using Image-Pro Plus 6.0.

MRI

In-vivo MRI was performed on a horizontal 11.7 Tesla MR scanner (Bruker Biospin) with a triple-axis gradient (maximum gradient strength=74 Gauss/cm). During imaging, mice were anesthetized with isoflurane (1%) in room air and oxygen mixed at 3:1 ratio *via* a vaporizer, and positioned in an animal holder containing circulating warm water (Bruker Biospin). Respiration was monitored *via* a pressure sensor (SAII, Stony Brook) and maintained at 40-60 breath/min. After imaging, animals recovered within 5 min.

Image acquisition was performed using a quadrature transmit volume coil (70-mm diameter) and a 4-channel mouse brain receive-only phased array coil (Bruker Biospin). Multi-slice T2-weighted images were acquired using the rapid acquisition with refocused echoes (RARE) sequence with an echo time (TE) of 50 ms, a repetition time (TR) of 3600 ms, four signal averages, echo train length of eight, field of view (FOV) of 15x15 mm, 32 slices, and a native resolution of 0.078x0.078x0.50 mm.

Erichrome cyanin staining

Slides were oven-dried at 50°C for 3 h, hydrated in 95% and 70% ethanol. After rinsing with distilled water twice, the sections were stained with an erichrome cyanine solution consisting of 0.4% $FeCl_3$, 0.2% erichrome cyanine (Sigma-Aldrich) and 0.5% H_2SO_4. Section development was performed by alternating exposure to 0.1% NH_4OH for 3-7 s and rinsing in distilled water for 30 s until the blue background was reduced and cells turned faintly pink but still had blue shading. After the last rinse in water, sections were dehydrated in 70%, 95%, and

100% ethanol (two changes), and three changes of xylene for 10 min each before being processed for microscopy.

Transmission electron microscopy and g-ratio measurement

Perfused shiverer mouse brains were placed under a fluorescent dissection microscope. A 3-mm diameter cube was dissected from the mGRP transplanted corpus callosum and fixed in 4% glutaraldehyde following postfixation in OsO_4, and embedded in Epon. Thin sections of 70 nm were stained with citrate/uranyl acetate as recently described (Lyczek *et al.*, 2017). Images were acquired using a Zeiss Libra transmission electron microscope from the upper left field and then, in a "zigzag" fashion with equidistant movement. G-ratio was measured as inner/outer diameter of the myelin sheath (300 axons per animal).

MiRNA in situ hybridization

In situ hybridization (ISH) for miR-223 and miR-146 (miRCURY LNA miRNA probes, Exiqon) was performed using miRCURY LNA microRNA ISH Kit (Exiqon) according to manufacturer's protocol. In brief, cryosections were air dried at room temperature and treated with Proteinase-K for 10 min, washed twice in PBS. Hybridization mix was then applied for 60 min at 52°C following washes in descending concentrations of SSC buffers. Next, sections were incubated sequentially in blocking solution for 15 min and anti-DIG reagent conjugated with rhodamine (Roche) for 60 min. After three washes with PBS and counterstained with DAPI, slides were mounted with Floro-Gel Mounting Media (EMS) and imaged with ZEISS AX10

fluorescence microscope.

Supplementary Figures and Figure legends

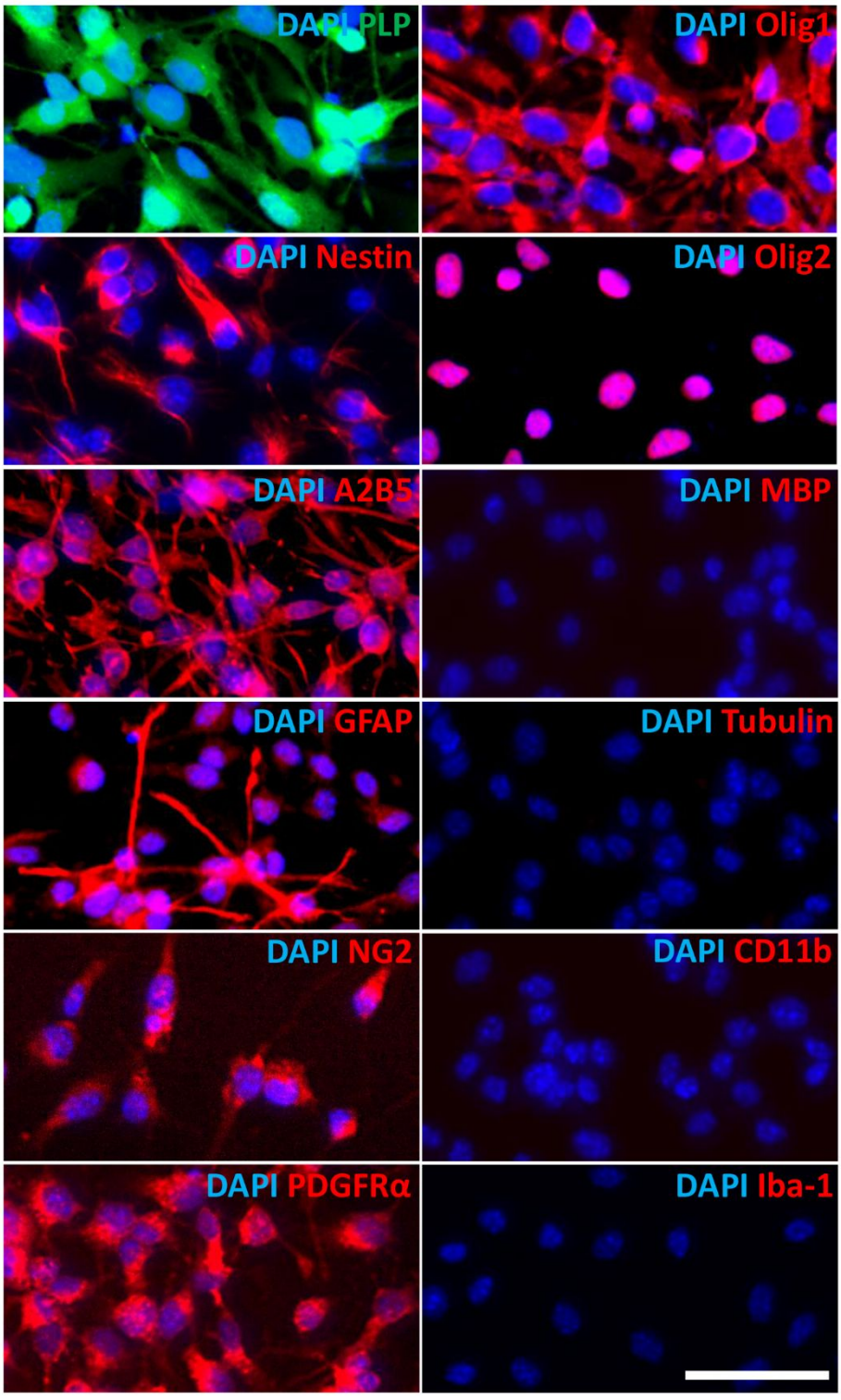

Supplementary Fig. 1. Spinal cord-derived mGRPs express macroglial lineage but not neuronal markers. PLP-GFP positive mGRP cells were isolated from E13.5 mouse spinal cord and cultured in selection medium for 10 days. Immunocytochemistry was performed against multiple marker antigens indicated at the upper right corners of each images. Scale bar: 50 μm.

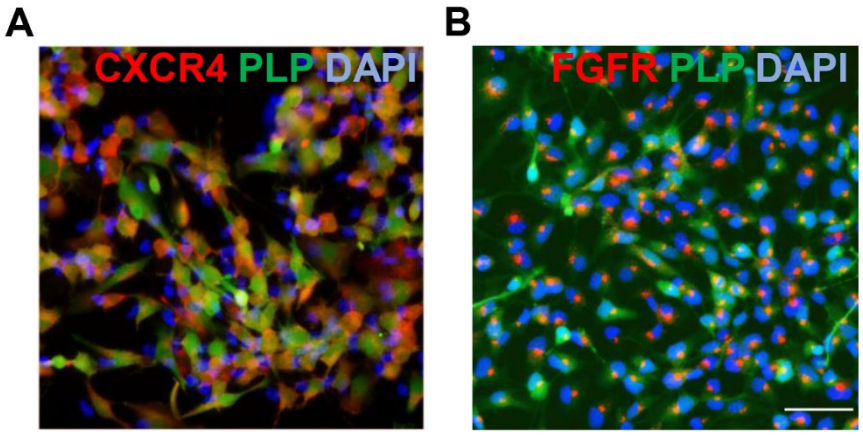

Supplementary Fig. 2. Immunocytochemistry for migration-mediating molecules. PLP-GFP positive mGRP cells were isolated from E13.5 mouse spinal cord and cultured in selection medium for 10 days. Immunocytochemistry was performed with (**A**) CXCR4 and (**B**) FGFR antibodies. Scale bar: 50 μm.

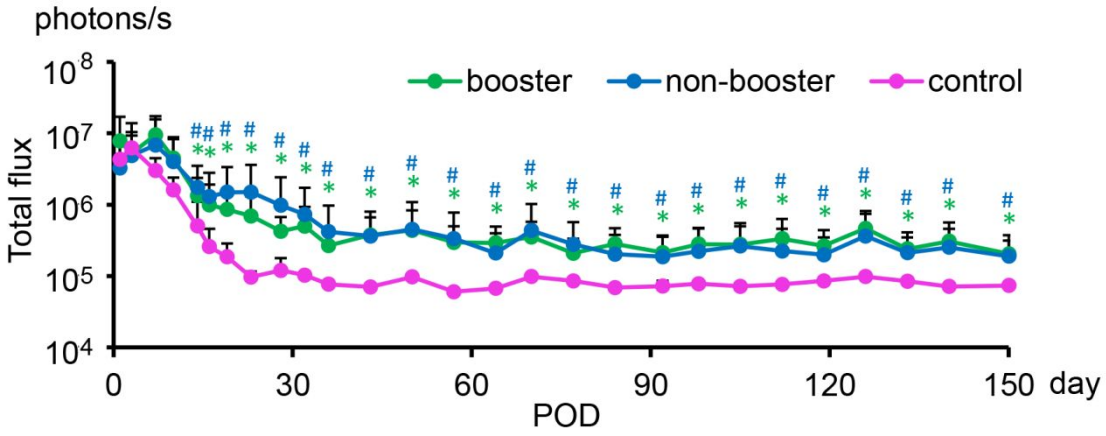

Supplementary Fig. 3. Additional CTLA4-Ig application does not further enhance graft survival. Logarithmic BLI values of non-booster group (MR-1 and CTLA4-Ig treatment on

POD0, 2, 4, 6, n=5), booster group (additional CTLA4-Ig application on POD30, 60, 90, n=5), and control group of B6 mice (n=5) that received intracerebral mGRP transplantation. There was no statistical difference between booster and non-booster group at any time point examined. Both booster (*, $p<0.05$) and non-booster group BLI signals ($^{\#}$, $p<0.05$) were significantly higher than in the control group from POD14 onwards. Regression analysis was reported as type III tests of fixed effects, with the lowest mean square (LMS) difference test used for comparison between means (PROC MIXED, SAS 9.2). A coefficient of determination was calculated, and the BLI data were subjected to logistic transformation to maximize the model fit.

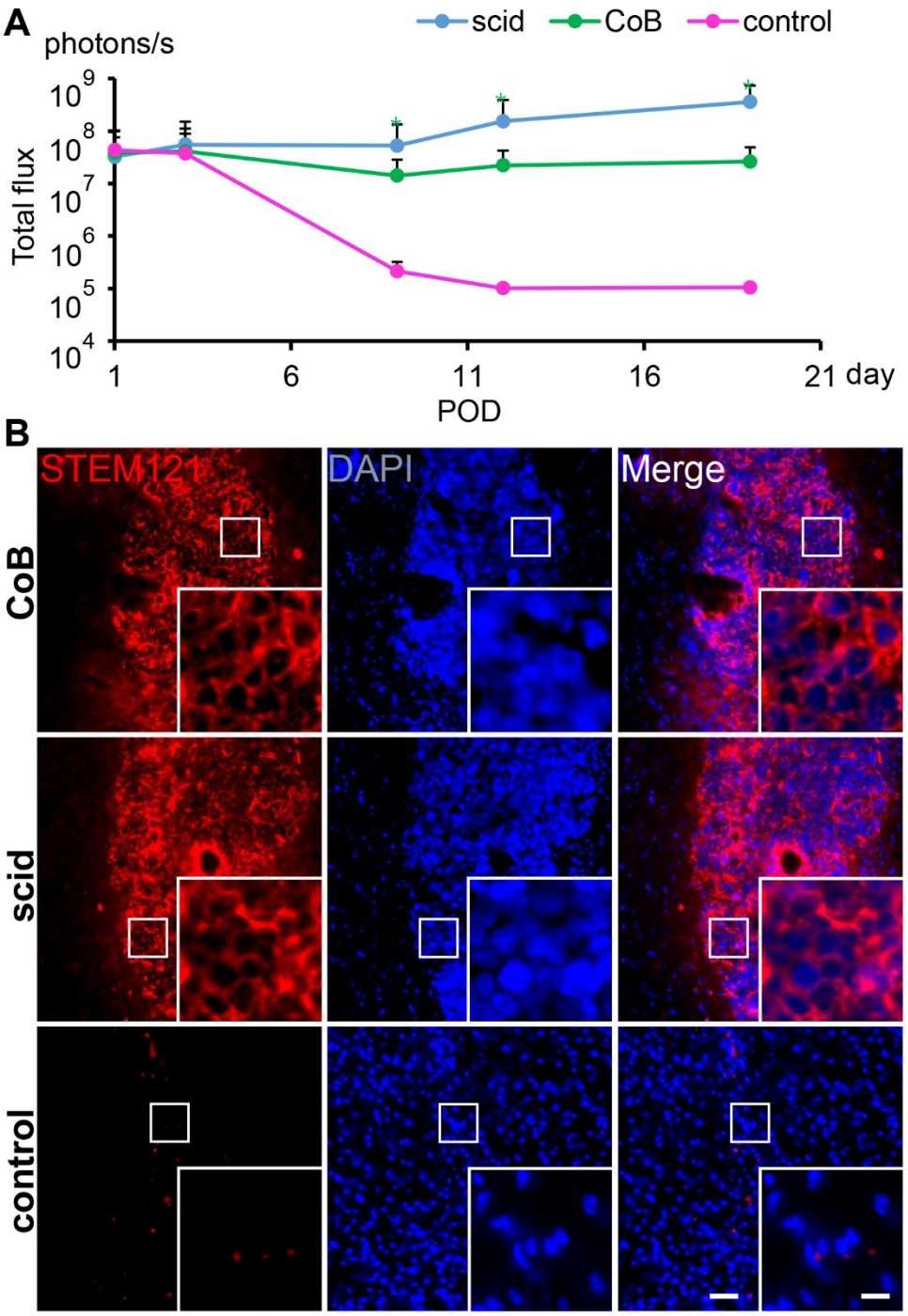

Supplementary Fig. 4. Costimulation blockade protects xenogeneic GRPs from immune rejection. (**A**) Intracerebral hGRP engrafted B6 mice were subjected to longitudinal BLI and the logarithmic total flux over their heads were plotted. The statistically significant difference between CoB and control group (*, $p<0.05$, n=5) started from POD9 and lasted till POD19. There were no BLI signal differences between CoB and scid groups ($p>0.4$, n=5). Regression

analysis was reported as type III tests of fixed effects, with the lowest mean square (LMS) difference test used for comparison between means (PROC MIXED, SAS 9.2). A coefficient of determination was calculated, and the BLI data were subjected to logistic transformation to maximize the model fit. (**B**) Immunohistochemistry on B6 and scid mouse brain specimens was performed with STEM121 antibodies and DAPI staining on POD19. Scale bar: 100/10 µm in low/high magnificent images.

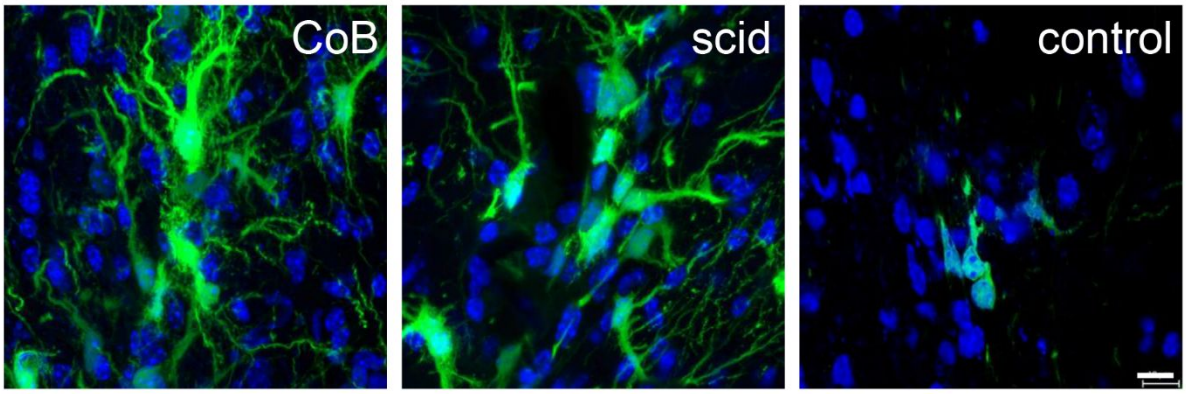

Supplementary Fig. 5. GRPs are vital after 19 days of intracerebral transplantation with costimulation blockade treatment. Confocal microscopy for PLP-GFP positive mGRPs being transplanted into CoB, scid and control mouse brains on POD19. Cell nuclei were stained with DAPI. Note that mGRPs extended complex processes in CoB and scid brains indicating the integration into host brains, but displayed moribund morphology in control brains. Scale bar: 10 µm.

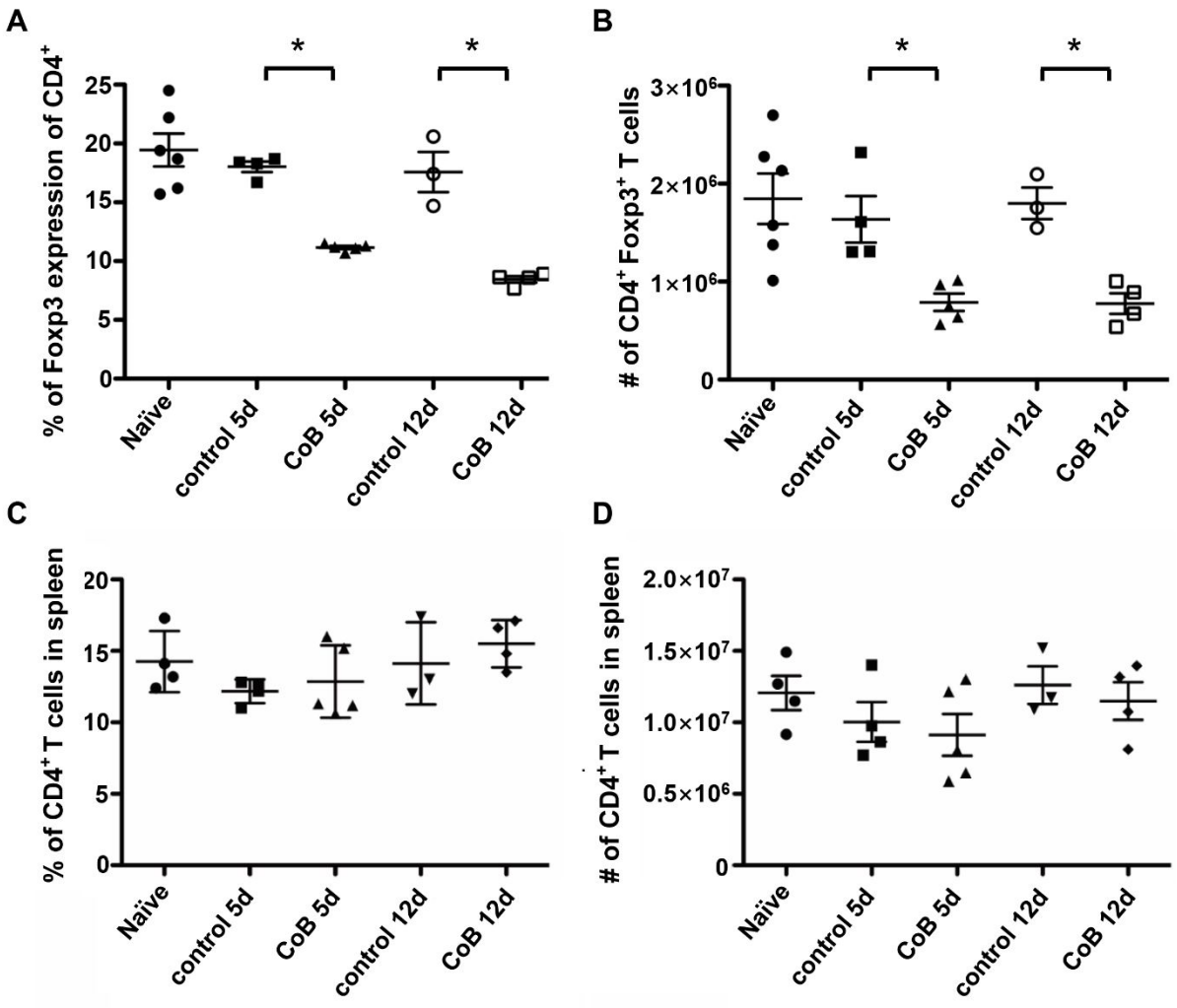

Supplementary Fig. 6. Peripheral Treg population is decreased in costimulation blockade treated mice. T cells isolated from naïve, control and CoB B6 mouse spleens were analyzed for the proportion (**A**) and absolute number (**B**) of $CD4^+$, $FoxP3^+$ Tregs by flow cytometry. Control mice had significantly more Tregs residing in the spleen than CoB mice on both POD5 ($p<0.0001$) and POD12 ($p=0.0016$). There was no difference in neither $CD4^+$ cell proportion (**C**) nor absolute numbers (**D**). Independent two sample *t*-test (SPSS 22.0).

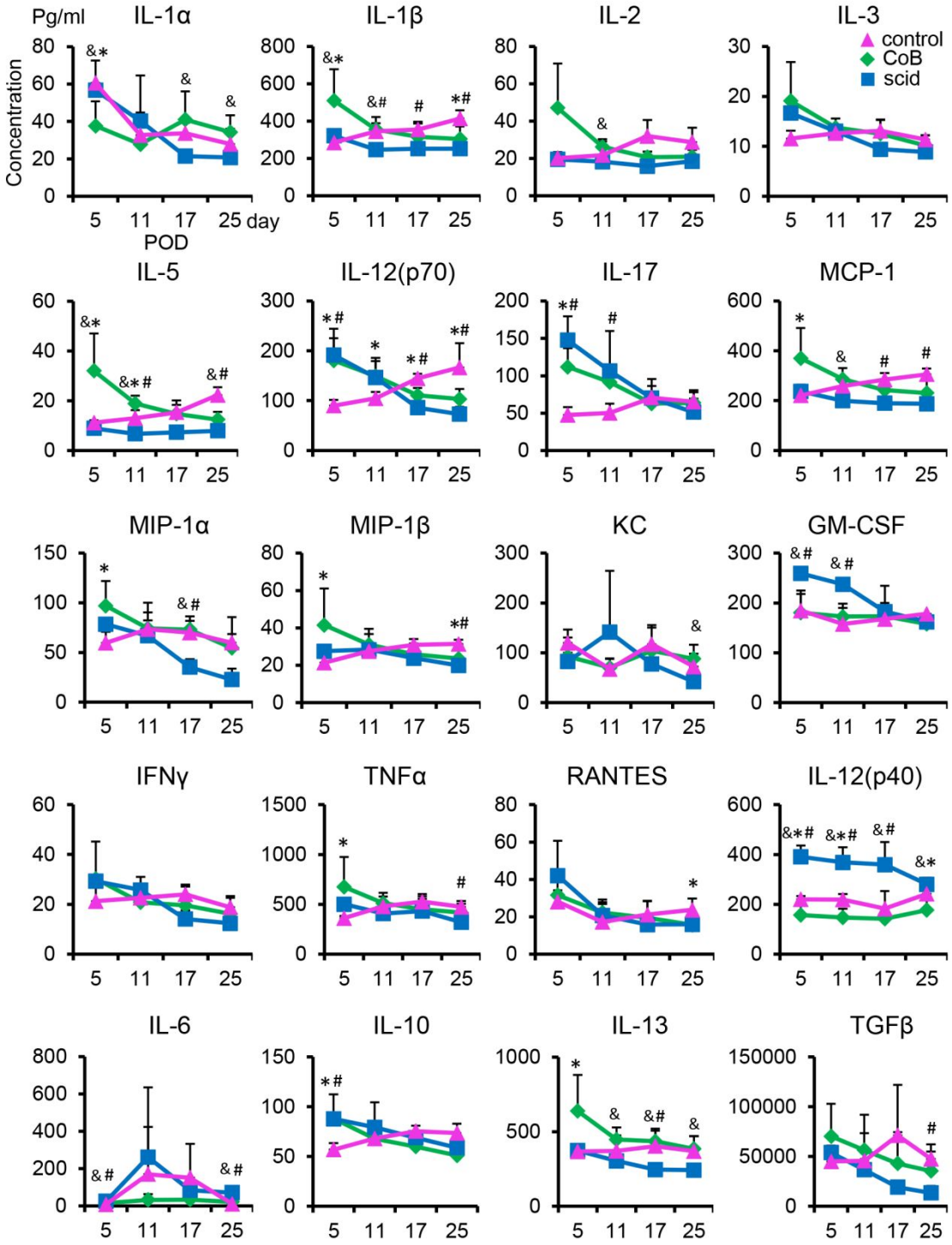

Supplementary Fig. 7. Costimulation blockade mitigates the post-transplantation pro-inflammation cytokine profile. Sera from intracerebrally mGRP transplanted CoB, control, and scid mice were drawn on POD5, 11, 17, 25 and subjected to a high throughput cytokine analysis. Cytokines that were within the detection range are presented with absolute values and standard deviation at different time points examined. One-way ANOVA with LSD *post hoc*

corrections. *p<0.05 between CoB and control mice, &p<0.05 between CoB and scid mice, #p<0.05 between scid and control mice (n=5 in each group).

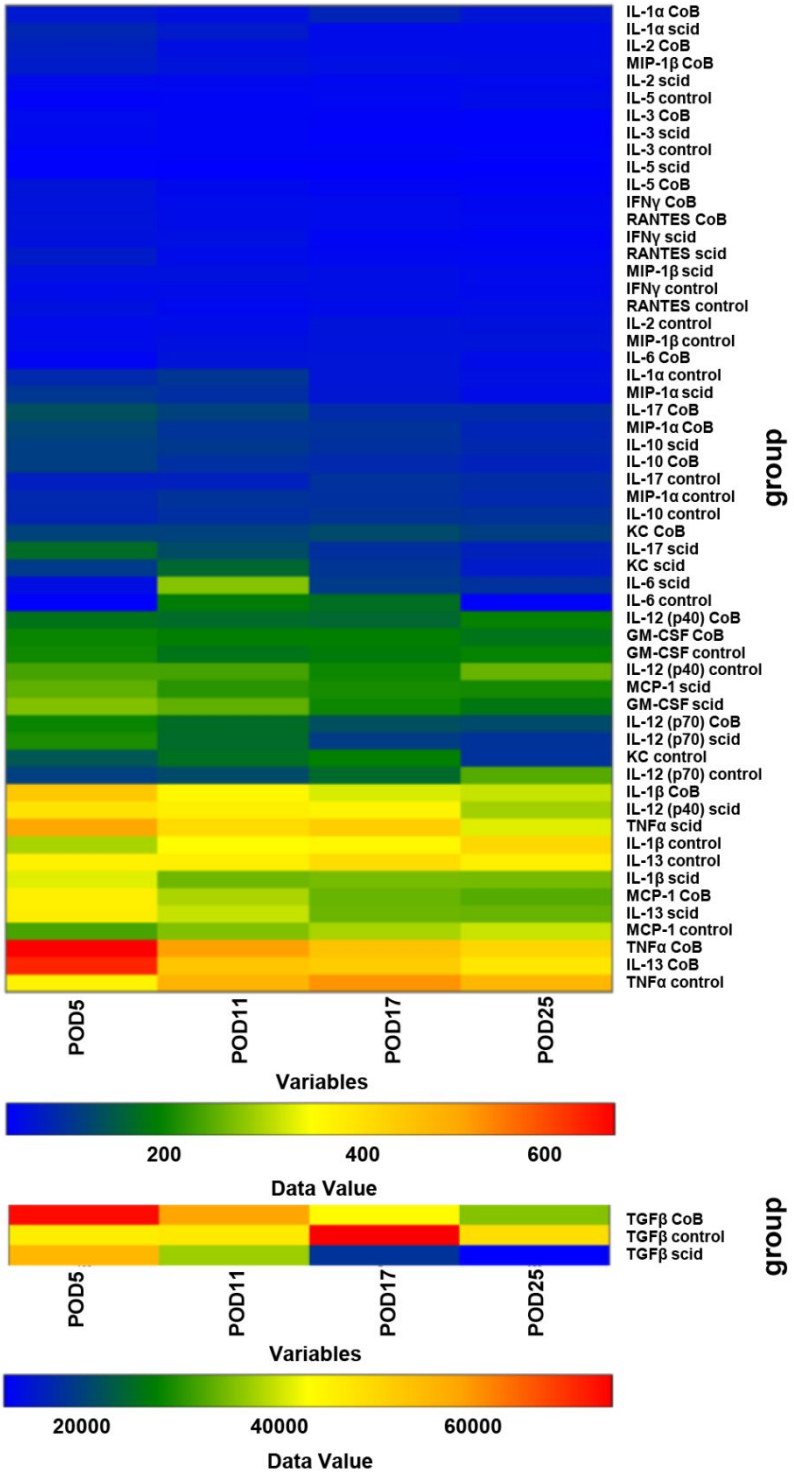

Supplementary Fig. 8. Clustered heatmaps of the serum cytokines after intracerebral mGRP transplantation. Sera from intracerebral mGRP transplanted CoB, control, and scid

mice were drawn on POD5, 11, 17, 25 and subjected to a high throughput cytokine analysis. Cluster analysis was performed with NCSS Statistical Software based on the quantitative data presented in Supplementary Fig. 7.

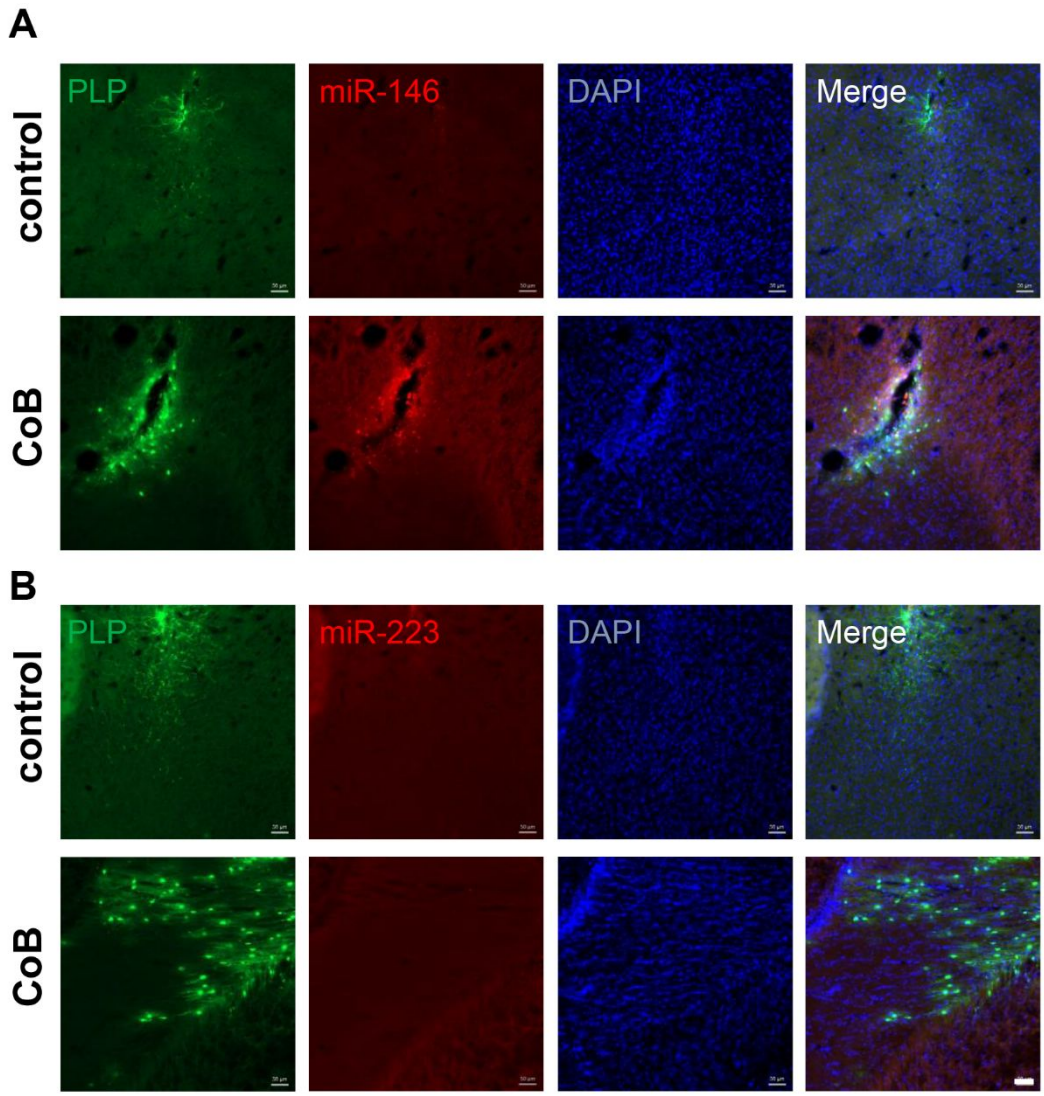

Supplementary Fig. 9. Costimulation blockade upregulates intragraft miR-146 expression post mGRP transplantation. *In situ* miRNA hybridization with DAPI counterstaining was performed for mGRP transplanted CoB and control mouse brains on POD19. (**A**) Mouse brain cryosections were hybridized with miR-146 probes and note its increased expression co-localizing with mGRPs in CoB brains. Control brains were negative for miR-146 hybridization.

(**B**). Mouse brain cryosections were hybridized with miR-223 probes. There was no positive hybridization in neither CoB nor control brains. Scale bar: 50 μm.

Supplementary Table 1. GFP-MBP co-localization parameters.

	Manders' overlap coefficient, R	colocalization coefficient, m1	colocalization coefficient, m2
shiverer-CoB 33d	0.5316±0.1325	0.5793±0.2078	0.9448±0.0468
shiverer-CoB 90d	0.4335±0.1880	0.7489±0.1291	0.8629±0.0917
shiverer-rag2 90d	0.4352±0.1081	0.5355±0.2279	0.8749±0.0929

References:

Lyczek A, Arnold A, Zhang J, Campanelli JT, Janowski M, Bulte JW, et al. Transplanted human glial-restricted progenitors can rescue the survival of dysmyelinated mice independent of the production of mature, compact myelin. Exp Neurol 2017; 291: 74-86.

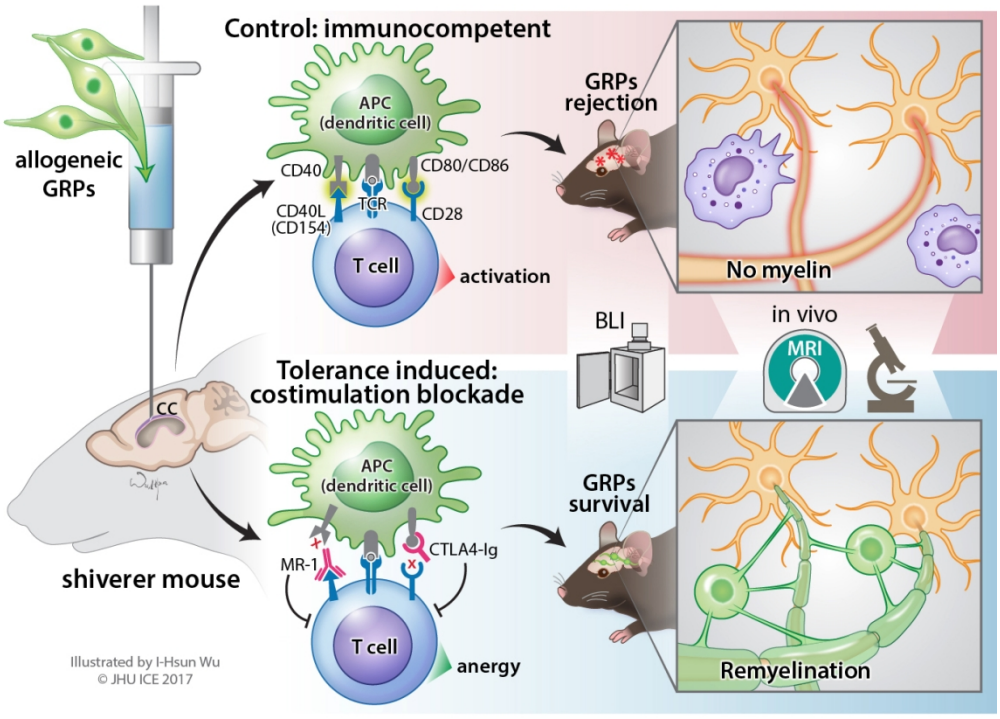

116x83mm (300 x 300 DPI)

The ARRIVE Guidelines Checklist

Animal Research: Reporting In Vivo Experiments

Carol Kilkenny[1], William J Browne[2], Innes C Cuthill[3], Michael Emerson[4] and Douglas G Altman[5]

[1]The National Centre for the Replacement, Refinement and Reduction of Animals in Research, London, UK, [2]School of Veterinary Science, University of Bristol, Bristol, UK, [3]School of Biological Sciences, University of Bristol, Bristol, UK, [4]National Heart and Lung Institute, Imperial College London, UK, [5]Centre for Statistics in Medicine, University of Oxford, Oxford, UK.

	ITEM	RECOMMENDATION	Section/ Paragraph
Title	1	Provide as accurate and concise a description of the content of the article as possible.	√Page 1
Abstract	2	Provide an accurate summary of the background, research objectives, including details of the species or strain of animal used, key methods, principal findings and conclusions of the study.	√Page 2
INTRODUCTION			
Background	3	a. Include sufficient scientific background (including relevant references to previous work) to understand the motivation and context for the study, and explain the experimental approach and rationale. b. Explain how and why the animal species and model being used can address the scientific objectives and, where appropriate, the study's relevance to human biology.	√Page 4-6
Objectives	4	Clearly describe the primary and any secondary objectives of the study, or specific hypotheses being tested.	√Page 6
METHODS			
Ethical statement	5	Indicate the nature of the ethical review permissions, relevant licences (e.g. Animal [Scientific Procedures] Act 1986), and national or institutional guidelines for the care and use of animals, that cover the research.	√Page 13-14
Study design	6	For each experiment, give brief details of the study design including: a. The number of experimental and control groups. b. Any steps taken to minimise the effects of subjective bias when allocating animals to treatment (e.g. randomisation procedure) and when assessing results (e.g. if done, describe who was blinded and when). c. The experimental unit (e.g. a single animal, group or cage of animals). A time-line diagram or flow chart can be useful to illustrate how complex study designs were carried out.	√Page 7-13, Table 1, Supplementary methods
Experimental procedures	7	For each experiment and each experimental group, including controls, provide precise details of all procedures carried out. For example: a. How (e.g. drug formulation and dose, site and route of administration, anaesthesia and analgesia used [including monitoring], surgical procedure, method of euthanasia). Provide details of any specialist equipment used, including supplier(s). b. When (e.g. time of day). c. Where (e.g. home cage, laboratory, water maze). d. Why (e.g. rationale for choice of specific anaesthetic, route of administration, drug dose used).	√Page 7-13, Supplementary methods
Experimental animals	8	a. Provide details of the animals used, including species, strain, sex, developmental stage (e.g. mean or median age plus age range) and weight (e.g. mean or median weight plus weight range). b. Provide further relevant information such as the source of animals, international strain nomenclature, genetic modification status (e.g. knock-out or transgenic), genotype, health/immune status, drug or test naïve, previous procedures, etc.	√Page 7

The ARRIVE guidelines. Originally published in *PLoS Biology*, June 2010[1]

Housing and husbandry	9	Provide details of: a. Housing (type of facility e.g. specific pathogen free [SPF]; type of cage or housing; bedding material; number of cage companions; tank shape and material etc. for fish). b. Husbandry conditions (e.g. breeding programme, light/dark cycle, temperature, quality of water etc for fish, type of food, access to food and water, environmental enrichment). c. Welfare-related assessments and interventions that were carried out prior to, during, or after the experiment.	√Page 7
Sample size	10	a. Specify the total number of animals used in each experiment, and the number of animals in each experimental group. b. Explain how the number of animals was arrived at. Provide details of any sample size calculation used. c. Indicate the number of independent replications of each experiment, if relevant.	√Page 7-13, Table 1
Allocating animals to experimental groups	11	a. Give full details of how animals were allocated to experimental groups, including randomisation or matching if done. b. Describe the order in which the animals in the different experimental groups were treated and assessed.	√Page 7-13
Experimental outcomes	12	Clearly define the primary and secondary experimental outcomes assessed (e.g. cell death, molecular markers, behavioural changes).	√Page 7-13
Statistical methods	13	a. Provide details of the statistical methods used for each analysis. b. Specify the unit of analysis for each dataset (e.g. single animal, group of animals, single neuron). c. Describe any methods used to assess whether the data met the assumptions of the statistical approach.	√Page 13
RESULTS			
Baseline data	14	For each experimental group, report relevant characteristics and health status of animals (e.g. weight, microbiological status, and drug or test naïve) prior to treatment or testing. (This information can often be tabulated).	√Table 1, Page 15-22
Numbers analysed	15	a. Report the number of animals in each group included in each analysis. Report absolute numbers (e.g. 10/20, not 50%[2]). b. If any animals or data were not included in the analysis, explain why.	√Page 7, 15-22, Table 1
Outcomes and estimation	16	Report the results for each analysis carried out, with a measure of precision (e.g. standard error or confidence interval).	√Page 15-22 and figure legends
Adverse events	17	a. Give details of all important adverse events in each experimental group. b. Describe any modifications to the experimental protocols made to reduce adverse events.	We did not see adverse events.
DISCUSSION			
Interpretation/ scientific implications	18	a. Interpret the results, taking into account the study objectives and hypotheses, current theory and other relevant studies in the literature. b. Comment on the study limitations including any potential sources of bias, any limitations of the animal model, and the imprecision associated with the results[2]. c. Describe any implications of your experimental methods or findings for the replacement, refinement or reduction (the 3Rs) of the use of animals in research.	√Page 23-27
Generalisability/ translation	19	Comment on whether, and how, the findings of this study are likely to translate to other species or systems, including any relevance to human biology.	√Page 23-27

Funding	20	List all funding sources (including grant number) and the role of the funder(s) in the study.	√Page 27

References:
1. Kilkenny C, Browne WJ, Cuthill IC, Emerson M, Altman DG (2010) Improving Bioscience Research Reporting: The ARRIVE Guidelines for Reporting Animal Research. *PLoS Biol* 8(6): e1000412. doi:10.1371/journal.pbio.1000412
2. Schulz KF, Altman DG, Moher D, the CONSORT Group (2010) CONSORT 2010 Statement: updated guidelines for reporting parallel group randomised trials. *BMJ* 340:c332.